Atmos. Chem. Phys., 15, 9819–9849, 2015
www.atmos-chem-phys.net/15/9819/2015/
doi:10.5194/acp-15-9819-2015

Atmospheric Chemistry and Physics
Open Access

Long-lived atmospheric trace gases measurements in flask samples from three stations in India

X. Lin[1], N. K. Indira[2], M. Ramonet[1], M. Delmotte[1], P. Ciais[1], B. C. Bhatt[3], M. V. Reddy[4], D. Angchuk[3], S. Balakrishnan[4], S. Jorphail[3], T. Dorjai[3], T. T. Mahey[3], S. Patnaik[4], M. Begum[5], C. Brenninkmeijer[6], S. Durairaj[5], R. Kirubagaran[7], M. Schmidt[1,8], P. S. Swathi[2], N. V. Vinithkumar[5], C. Yver Kwok[1], and V. K. Gaur[2]

[1]Laboratoire des Sciences du Climat et de l'Environnement (LSCE), UMR CEA-CNRS-UVSQ, Gif-sur-Yvette 91191, France
[2]CSIR Fourth Paradigm Institute (formerly CSIR Centre for Mathematical Modelling and Computer Simulation), NAL Belur Campus, Bengaluru 560 037, India
[3]Indian Institute of Astrophysics, Bengaluru 560 034, India
[4]Department of Earth Sciences, Pondicherry University, Puducherry 605 014, India
[5]Andaman and Nicobar Centre for Ocean Science and Technology (ANCOST), ESSO-NIOT, Port Blair 744103, Andaman and Nicobar Islands, India
[6]Max Planck Institute for Chemistry, Hahn-Meitner-Weg 1, 55128 Mainz, Germany
[7]Earth System Sciences Organisation – National Institute of Ocean Technology (ESSO-NIOT), Ministry of Earth Sciences, Government of India, Tamil Nadu, Chennai 600 100, India
[8]Institut für Umweltphysik, Universität Heidelberg, INF 229, 69120 Heidelberg, Germany

Correspondence to: X. Lin (xin.lin@lsce.ipsl.fr)

Received: 26 January 2015 – Published in Atmos. Chem. Phys. Discuss.: 10 March 2015
Revised: 11 August 2015 – Accepted: 17 August 2015 – Published: 1 September 2015

Abstract. With the rapid growth in population and economic development, emissions of greenhouse gases (GHGs) from the Indian subcontinent have sharply increased during recent decades. However, evaluation of regional fluxes of GHGs and characterization of their spatial and temporal variations by atmospheric inversions remain uncertain due to a sparse regional atmospheric observation network. As a result of an Indo-French collaboration, three new atmospheric stations were established in India at Hanle (HLE), Pondicherry (PON) and Port Blair (PBL), with the objective of monitoring the atmospheric concentrations of GHGs and other trace gases. Here we present the results of the measurements of CO_2, CH_4, N_2O, SF_6, CO, and H_2 from regular flask sampling at these three stations over the period 2007–2011. For each species, annual means, seasonal cycles and gradients between stations were calculated and related to variations in natural GHG fluxes, anthropogenic emissions, and monsoon circulations. Covariances between species at the synoptic scale were analyzed to investigate the likely source(s) of emissions. The flask measurements of various trace gases at the three stations have the potential to constrain the inversions of fluxes over southern and northeastern India. However, this network of ground stations needs further extension to other parts of India to better constrain the GHG budgets at regional and continental scales.

1 Introduction

Since pre-industrial times, anthropogenic greenhouse gas (GHG) emissions have progressively increased the radiative forcing of the atmosphere, leading to impacts on the climate system and human society (IPCC, 2013, 2014a, b). With rapid socioeconomic development and urbanization during recent decades, a large and growing share of GHG emissions is contributed by emerging economies like China and India. In 2010, India became the world's third largest GHG emitter, after China and the USA (EDGAR v4.2, 2011; Le Quéré et al., 2015). Between 1991 and 2010, anthropogenic GHG emissions in India increased by $\sim 100\,\%$ from 1.4 to 2.8 $GtCO_2eq$, much faster than rates of most developed countries and economies like the USA (9 %) and EU ($-14\,\%$)

over the same period (EDGAR v4.2, 2011). Without systematic efforts at mitigation, this trend will continue in the coming decades, given that the per capita emission rate in India is still much lower than that of the more developed countries. For comparison, in 2010, the per capita GHG emission rates were 2.2, 10.9, 17.6, and 21.6 t CO_2eq capita^{-1} for India, the UK, Russia, and the USA, respectively (EDGAR v4.2, 2011). In particular, non-CO_2 GHG emissions are substantial in India, most of which are contributed by agricultural activities over populous rural areas (Pathak et al., 2010). In 2010, anthropogenic CH_4 and N_2O emissions in India amounted to 29.6 TgCH_4 ($\approx$ 0.62 GtCO_2eq) and 0.8 Tg N_2O ($\approx$ 0.23 GtCO_2eq), together accounting for 32 % of the country's anthropogenic GHG emissions, of which contributions of the agricultural sector were 60 and 73 %, respectively (EDGAR v4.2, 2011). Reducing emissions of these two non-CO_2 GHGs may offer a more cost-effective way to mitigate future climate change than by attempting to directly reduce CO_2 emissions (Montzka et al., 2011).

Effective climate mitigation strategies need accurate reporting of sources and sinks of GHGs. This is also a requirement of the United Nations Framework Convention on Climate Change (UNFCCC). Current estimates of GHG budgets in India, either from the top-down approaches (based on atmospheric inversions) or bottom-up approaches (based on emission inventories or biospheric models), have larger uncertainties than for other continents. For instance, Patra et al. (2013) reported a net biospheric CO_2 sink of -104 ± 150 TgC yr^{-1} over South Asia during 2007–2008 based on global inversions from 10 TransCom CO_2 models (Peylin et al., 2013) and a regional inversion (Patra et al., 2011b), while the bottom-up approach gave an estimate of -191 ± 193 TgC yr^{-1} over the period of 2000–2009 (Patra et al., 2013). Notably, these estimates have uncertainties as high as 100–150 %, much larger compared to those of Europe ($\sim$ 30 %, see Luyssaert et al., 2012) and North America ($\sim$ 60 %, see King et al., 2015), where observational networks are denser and emission inventories are more accurate. Evaluation of N_2O emissions from five TransCom N_2O inversions also exhibited the largest differences over South Asia (Thompson et al., 2014b). A main source of uncertainty is the lack of atmospheric observation data sets with sufficient temporal and spatial coverage (Patra et al., 2013; Thompson et al., 2014b). Networks of atmospheric stations that were used to constrain estimates of global GHG fluxes show gaps over South Asia (Patra et al., 2011a; Thompson et al., 2014b, c; Peylin et al., 2013), with Cape Rama (CRI – 15.08° N, 73.83° E, 60 m a.s.l.) on the southwest coast of India being the only Indian station (Rayner et al., 2008; Patra et al., 2009; Tiwari et al., 2011; Bhattacharya et al., 2009; Saikawa et al., 2014). Recently a few other ground stations have been established in western India and the Himalayas to monitor GHGs and atmospheric pollutants, which are located in Sinhagad (SNG – 18.35° N, 73.75° E, 1600 m a.s.l.; Tiwari and Kumar, 2012; Tiwari et al., 2014), Mount Abu (24.60° N, 72.70° E, 1700 m a.s.l.; S. Lal, personal communication, 2015), Ahmedabad (23.00° N, 72.50° E, 55 m a.s.l.; Lal et al., 2015), Nainital (29.37° N, 79.45° E, 1958 m a.s.l.; Kumar et al., 2010) and Darjeeling (27.03° N, 88.15° E, 2194 m a.s.l.; Ganesan et al., 2013). Most of these stations started to measure atmospheric GHG concentrations very recently (e.g., Sinhagad – since 2009; Ahmedabad – since 2013; Mount Abu – since 2013; Nainital – since 2006; Darjeeling – since 2011), and data sets are not always available. In addition, aircraft and satellite observations have also been carried out and provided useful constraints on estimates of GHG fluxes in this region (Park et al., 2007; Xiong et al., 2009; Schuck et al., 2010; Patra et al., 2011b; Niwa et al., 2012; Zhang et al., 2014). Although inclusion of measurements from South Asia significantly reduces uncertainties in top-down estimates of regional GHG emissions (e.g., Huang et al., 2008; Niwa et al., 2012; Zhang et al., 2014), a denser atmospheric observational network with sustained measurements is still needed over this vast and fast-growing region for an improved, more-detailed, and necessary understanding of GHG budgets.

Besides the lack of a comprehensive observational network, the seasonally reversing Indian monsoon circulations and orographic effects complicate simulation of regional atmospheric transport, which contributes to the uncertainty of inverted GHG fluxes (e.g., Thompson et al., 2014b). The Indian monsoon system is a prominent meteorological phenomenon in South Asia, which, at lower altitudes, is characterized by strong southwesterlies from the Arabian Sea to the Indian subcontinent during the boreal summer, and by northeasterlies during the boreal winter (Goswami, 2005). The summer monsoon is associated with deep convection, which mixes the boundary layer air into the upper troposphere and lower stratosphere (Schuck et al., 2010; Lawrence and Lelieveld, 2010). Little deep convection occurs over South Asia during the winter monsoon period, which carries less moisture (Lawrence and Lelieveld, 2010). The Indian monsoon also impacts biogenic activities (e.g., vegetation growth, microbial activity) and GHG fluxes through its effects on rainfall variations (Tiwari et al., 2013; Valsala et al., 2013; Gadgil, 2003). Given that accurate atmospheric transport is critical for retrieving reliable inversion of GHG fluxes, an observational network that cover a range of altitudes including monitoring stations in mountainous regions would be valuable for validating and improving atmospheric transport models.

Since the 2000s, three new atmospheric ground stations have been established in India as part of the Indo-French collaboration, with the objective of monitoring the atmospheric concentrations of major GHGs and other trace gases in flask air samples. Of the three Indian stations, Hanle (HLE) is a high-altitude station situated in the western Indian Himalayas, while Pondicherry (PON) and Port Blair (PBL) are tropical surface stations located respectively on the southeastern coast of southern India and on an oceanic island in

the southeastern Bay of Bengal. In this study, we briefly describe the main features of these stations and present time series of flask air sample measurements of multiple trace gases at HLE, PON, and PBL over the period 2007–2011. Descriptions of the three stations as well as methods used to analyze and calibrate the flask measurements are given in Sect. 2. For each station, we measure the atmospheric concentrations of four major GHG species (CO_2, CH_4, N_2O and SF_6) and two additional trace gases (CO and H_2). Among these trace gases, CO_2, CH_4 and N_2O are the three most abundant GHGs in the atmosphere, and the UNFCCC requires each Non-Annex I Party to regularly report anthropogenic emissions of these gases (MoEF, 2012). Sulfur hexafluoride (SF_6) is widely considered a good tracer for anthropogenic activities with a long atmospheric lifetime and almost purely anthropogenic sources (Maiss et al., 1996), and the Non-Annex I Parties are also encouraged to provide information on their anthropogenic emissions (MoEF, 2012). Although CO and H_2 are not GHGs by themselves, both of them play critical roles in the CH_4 budgets through reaction with the free OH radicals (Ehhalt and Rohrer, 2009). Additionally, CO and H_2 are good tracers for biomass/biofuel burning (Andreae and Merlet, 2001), an important source of GHG emissions that is quite extensive in India (Streets et al., 2003b; Yevich and Logan, 2003). Time series of atmospheric concentrations of all these trace gases are analyzed for each station to characterize the annual means and seasonal cycles, with results and discussions presented in Sect. 3. Gradients between different stations are interpreted in the context of regional flux patterns and monsoon circulations (Sect. 3.1). We examine synoptic variations of CO_2, CH_4 and CO by analyzing the co-variances between species, using deviations from their smoothed fitting curves (Sect. 3.2). Finally, we investigate two abnormal CH_4 and CO events at PBL and propose likely sources and origins (Sect. 3.3). A summary of the paper and conclusions drawn from these results are given in Sect. 4.

2 Sampling stations and methods

2.1 Sampling stations

Figures 1 and S1 in the Supplement show the locations of HLE, PON, and PBL. We also present 5-day back trajectories from each station for all sampling dates in April–June (AMJ), July–September (JAS), October–December (OND) and January–March (JFM), respectively (Fig. 1a). Note that this four-period classification scheme is slightly different from the climatological seasons defined by the India Meteorological Department (IMD; Attri and Tyagi, 2010), in which months of a year are categorized into the pre-monsoon season (March–May), SW monsoon season (June–September), post-monsoon season (October–December) and the winter season (January and February). We adapted the IMD classification to facilitate better display and further analyses (e.g., Sect. 3.2), making sure that samples are fairly evenly distributed across all seasons. The back trajectories were generated using the Hybrid Single Particle Lagrangian Integrated Trajectory (HYSPLIT4) model (Draxler and Rolph, 2003), driven by wind fields from the Global Data Assimilation System (GDAS) archive data based on National Centers for Environmental Prediction (NCEP) model output (https://ready.arl.noaa.gov/gdas1.php).

The Hanle (HLE) station (32.780° N, 78.960° E, 4517 m a.s.l.) is located at the campus of the Indian Astronomical Observatory (IAO) atop Mt. Saraswati, about 300 m above the Nilamkhul Plain in the Hanle Valley of southeastern Ladakh in the northwestern Himalayas. The station was established in 2001 as a collaborative project between the Indian Institute of Astrophysics and LSCE, France. The flask sampling inlet is installed on the top of a 3 m mast fixed on the roof of a 2 m high building, and the ambient air is pumped through a Dekabon tubing with an outer diameter of $1/4''$. The area around the station is a cold mountain desert, with sparse vegetation and a small population of $\sim$1700 distributed over an area of $\sim 20\,km^2$. Anthropogenic activities are limited to small-scale crop production (e.g., barley and wheat) and livestock farming (e.g., yaks, cows, goats, and sheep). The nearest populated city of Leh (34.25° N, 78.00° E, 3480 m a.s.l.) with $\sim$27 000 inhabitants, lies 270 km to the northwest of this station. By virtue of its remoteness, high altitude, and negligible biotic and anthropogenic influences, HLE is representative of the background free tropospheric air masses in the northern mid-latitudes. Regular flask air sampling at this station has been operational since February 2004, and continuous in situ CO_2 measurements started in September 2005. Over the period 2007–2011, a total of 188 flask sample pairs were collected at HLE. Back trajectories show that HLE dominantly samples air masses that pass over northern Africa and the Middle East throughout the year, and those coming from South and Southeast Asia during the SW monsoon season (Fig. 1a). More detailed station information of HLE would be found in several earlier publications (Babu et al., 2011; Moorthy et al., 2011).

The Pondicherry (PON) station (12.010° N, 79.860° E, 20 m a.s.l) is located on the southeast coast of India, about 8 km north of the city of Pondicherry with a population of $\sim$240 000 (Census India, 2011). The station was established in collaboration with Pondicherry University in 2006. The flask sampling inlet, initially located on a 10 m mast fixed on the roof of the University Guest House, was later moved to a 30 m high tower in June, 2011. The ambient air is pumped from the top of the tower through a Dekabon tubing with an outer diameter of $1/4''$. The surrounding village Kalapet has a population of $\sim$9000 (Sivakumar and Anitha, 2012). A four-lane highway runs nearly 80 m to the west of the station with low traffic flow, especially during the nighttime, while the Indian Ocean stands about 100 m to the east of the station. Moreover, the two nearest megalopolises of Chen-

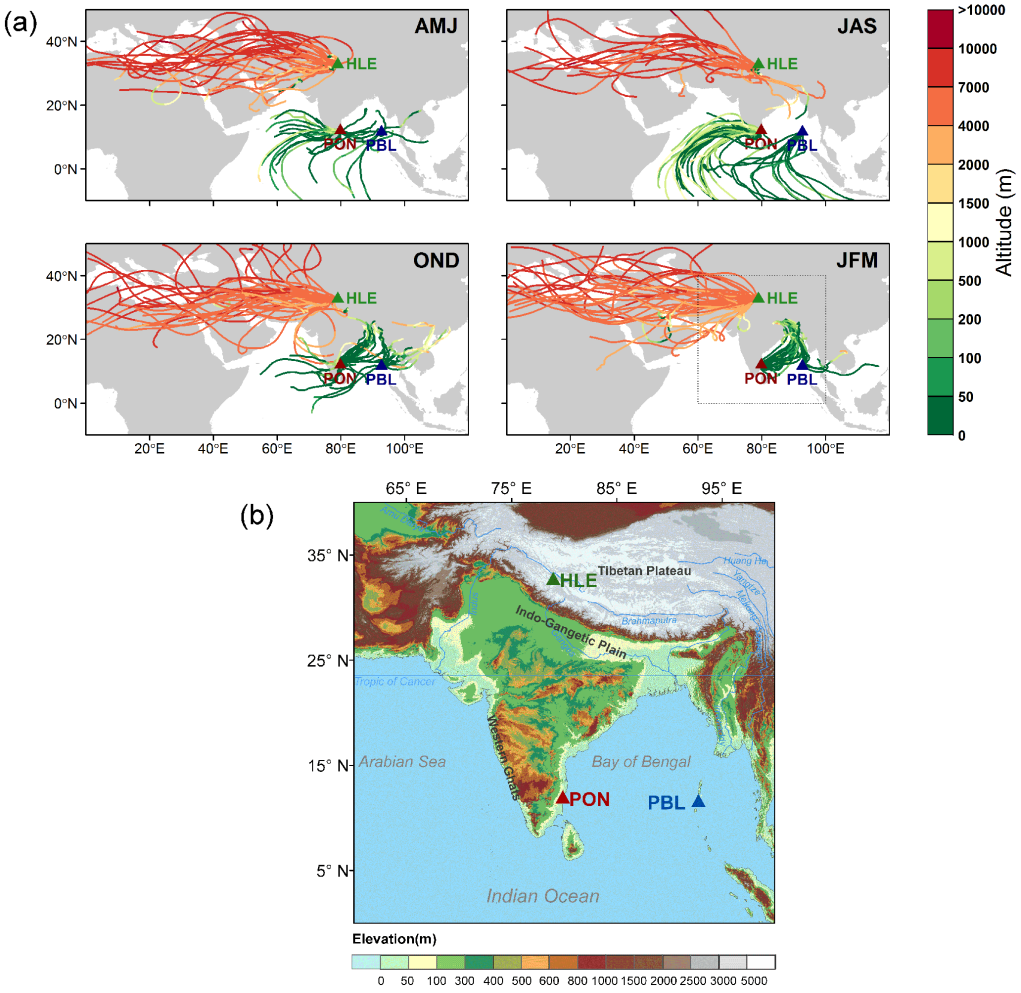

Figure 1. (a) Five-day back trajectories calculated for all sampling dates over the period 2007–2011 at Hanle (HLE), Pondicherry (PON), and Port Blair (PBL) during April–June (AMJ), July–September (JAS), October–December (OND) and January–March (JFM). Back trajectories are colored by the elevation of air masses at hourly time step. **(b)** Close-up terrain map from the box in **(a)**, showing locations of HLE, PON and PBL. The digital elevation data are obtained from NASA Shuttle Radar Topographic Mission (SRTM) product at 1km resolution (http://srtm.csi.cgiar.org).

nai and Bengaluru, both with populations of over 8 million (Census India, 2011), are approximately 143 km to the north and 330 km to the west of the station. Given its proximity to an urban area and a highway, PON could be influenced by local emissions. Although the highway nearby has low traffic flow, in situ measurements at PON (not presented in this paper) do show that this site is heavily polluted by local emissions during nighttime. In order to minimize the influences of local GHG sources/sinks, flask air sampling at PON is performed between 12:00 and 18:00 local time (LT) (actually 97 % of flask samples taken between 12:00 and 14:00 LT), when the sea breeze moves clean air masses towards the land and the boundary layer air is well mixed. Further, we also remove outliers that are likely polluted by local emissions and not representative of regional background concentrations (see Sect. 2.3.1 for details). We believe that through these two approaches the local influences at PON should be sufficiently minimized. Flask sampling at PON began in September 2006 and over the period 2007–2011, a total of 185 flask sample pairs were collected at the site. As shown in Fig. 1a, the air masses received at PON are strongly related to the monsoon circulations. During the boreal summer when the southwest monsoon prevails, PON is influenced by air masses originating from the Arabian Sea and southern India, whereas during the boreal winter, it receives air masses from the east and northeast parts of the Indian subcontinent, and the Bay of Bengal. During the boreal spring and autumn when the monsoon changes its direction, air masses of both origins are observed.

The Port Blair (PBL) station (11.650° N, 92.760° E, 20 m a.s.l.) is located on the small Andaman Islands in the southeastern Bay of Bengal, ∼1400 km east of PON, and

roughly 600 km west of Myanmar and Thailand. The station was established in collaboration with the National Institute of Ocean Technology (NIOT), India, and flask air sampling was initiated in July 2009. The flask sampling inlet is located on the top of a 30 m high tower, and the ambient air is pumped through a Dekabon tubing with an outer diameter of $1/4''$. The main city on the Andaman Islands, Port Blair, is about 8 km to the north of the station, with a population of $\sim 100\,000$ (Census India, 2011). Due to its proximity to vegetation and a small rural community, the station is not completely free from influences of local GHG fluxes. Therefore, flask samples at PBL are obtained in the afternoon between 13:00 and 15:00 LT, when the sea breeze moves towards the land, to minimize significant local influences. Over the period 2009–2011, a total of 63 flask sample pairs were collected at PBL. Back trajectories show that the air masses sampled at PBL are also controlled by the seasonally reversing monsoon circulations (Fig. 1a), with air masses from the Indian Ocean south of the Equator during the southwest monsoon season, and from the northeast part of the Indian subcontinent, the Bay of Bengal, and Southeast Asia during the northeast monsoon season. As for PON, air masses of both origins are detected at PBL during the boreal spring and autumn when the monsoon changes its direction.

2.2 Flask sampling and analysis

2.2.1 Flask sampling

In principle, flask samples are taken in pairs on a weekly basis at all three stations. However, in practice air samples are collected less frequently (on average every 10–12 days) due to bad meteorological conditions and technical problems. Whole air samples are filled into pre-conditioned 1 L cylindrical borosilicate glass flasks (Normag Labor und Prozesstechnik GmbH, Germany) with valves sealed by caps made from KEL-F (PTCFE) fitted at both ends. Additionally, a few flasks are equipped with valves sealed by the original Teflon PFA O-ring (Glass Expansion, Australia), accounting for ~ 5.0, 1.2 and 1.1 % of air samples respectively for HLE, PON and PBL during the study period. For the air samples stored in flasks sealed with the original Teflon PFA O-ring, corrections are made for the loss of CO_2 ($+0.0027$ ppm day^{-1}) and of N_2O ($+0.0035$ ppb day^{-1}) after analyses of the samples. The correction factors are empirically determined based on laboratory storage tests using flasks filled with calibrated gases. Drying of the air is performed using 10 g of magnesium perchlorate ($Mg(ClO_4)_2$) confined at each end with a glass wool plug in a stainless steel cartridge, located upstream of the pump unit. Tests have shown that use of the magnesium perchlorate drier does not result in any loss of the target compound. To prevent entrainment of material inside the sampling unit, a 7 µm filter is attached at the end of the cartridge. The flasks are flushed prior to sampling for 10–20 min at a rate of 4–5 L min^{-1}, and the air is compressed in the flasks to about 1 bar over the ambient pressure (pump: KNF Neuberger diaphragm pump powered by a 12 V DC motor, Germany, N86KNDC with EPDM membrane). The pressurizing process lasts for less than a minute.

2.2.2 Flask analyses

On average the flasks arrive at LSCE, France about 150 days after the sampling date. Leakage could occur during shipment, and any flask sample with too-low pressure is flagged in the analyses. Flask samples are analyzed for CO_2, CH_4, N_2O, SF_6, CO, and H_2 with two coupled gas chromatograph (GC) systems. The first gas chromatograph (HP6890, Agilent) is equipped with a flame ionization detector (FID) for CO_2 and CH_4 detection, and a standard electron capture detector (ECD) for N_2O and SF_6 detection. It is coupled with a second GC equipped with a reduced gas detector (RGD, Peak Laboratories, Inc., California, USA), for analyzing CO and H_2 via reduction of HgO and subsequent detection of Hg vapor through UV absorption. In the following paragraph we summarize the major configurations and parameters of the GC systems (also see Table S1 in the Supplement). Further details on the analyzer configuration are described in Lopez (2012) and Yver et al. (2009).

Both GC systems are composed of three complementary parts: the injection device, the separation elements and the detection sensors. As flask samples are already dried during sampling, they are only passed through a 5 mL glass trap maintained in an ethanol bath kept at -55 °C by a cryocooler (Thermo Neslab CC-65) to remove any remaining water vapor. The air samples are flushed with flask overpressure through a 15 mL sample loop for CO_2 and CH_4 analyses, a 15 mL sample loop for N_2O and SF_6 analyses, and a 1 mL sample loop for CO and H_2, at a flow rate of 200 mL min^{-1}. After temperature and pressure equilibration, the air sample is injected into the columns. The CO_2 and CH_4 separation is performed using a Hayesep-Q ($12' \times 3/16''$OD, mesh 80/100) analytical column placed in an oven at 80 °C, with a N_2 5.0 carrier gas at a flow rate of 50 mL min^{-1}. Detection of CH_4 and CO_2 (after conversion to CH_4 using a Ni catalyst and H_2 gas) is performed in the FID kept at 250 °C. The flame is fed with H_2 (provided by a NM-H_2 generator from F-DBS) at a flow rate of 100 mL min^{-1} and zero air (provided by a 75–82 zero air generator from Parker-Balston) at a flow rate of 300 mL min^{-1}. For N_2O and SF_6 separation, a Hayesep-Q ($4' \times 3/16''$ OD, mesh 80/100) pre-column and a Hayesep-Q ($6' \times 3/16''$ OD, mesh 80/100) analytical column, both placed in an oven at 80 °C, are used together with an Ar / CH_4 carrier gas at a flow rate of 40 mL min^{-1}. Detection of N_2O and SF_6 is performed in the ECD heated at 395 °C. For CO and H_2, we use a Unibeads 1S pre-column ($16.5'' \times 1/8''$ OD; mesh 60/80) to separate the two gases from the air matrix, and use a Molecular Sieve 5Å analytical column ($80'' \times 1/8''$ OD; mesh 60/80) to effectively sepa-

rate H_2 from CO. Both columns are placed in an oven kept at 105 °C. CO and H_2 are analyzed in the RGD detector heated to 265 °C. A measurement takes ∼ 5 min and calibration gases are measured at least every 0.45 h. For CO_2, CH_4, N_2O, and SF_6, we use two calibration gases, one with a high concentration and the other with a low concentration. The calibration and quality control cylinders are filled and spiked in a matrix of synthetic air containing N_2, O_2 and Ar prepared by Deuste Steininger (Germany). The concentration of the sample is calculated using a linear regression between the two calibration gases with a time interpolation between the two measurements of the same calibration gas (Messager, 2007; Lopez, 2012). For CO and H_2, we use only one standard and apply a correction for the nonlinearity of the analyzer (Yver et al., 2009; Yver, 2010). The nonlinearity is verified regularly with five calibration cylinders for CO and eight calibration cylinders for H_2. All the calibration gases themselves are determined against an international primary scale (CO_2: WMOX2007; CH_4: NOAA2004; N_2O: NOAA2005A; SF_6: NOAA2005; CO: WMOX2004; H_2: WMOX2009; Hall et al., 2007; Dlugokencky et al., 2005; Jordan and Steinberg, 2011; Zhao and Tans, 2006). Finally, a "target" gas is measured every 2 h after the calibration gases as a quality control of the scales and of the analyzers. The repeatability of the GC systems estimated from the target cylinder measurements over several days is 0.06 ppm for CO_2, 1 ppb for CH_4, 0.3 ppb for N_2O, 0.1 ppt for SF_6, 1 ppb for CO and 2 ppb for H_2. Additional quality control is made by checking the values of a flask target (a flask filled with calibrated gases) placed on each measurement sequence.

For both of the GC systems, data acquisition, valve shunting, and temperature regulation are entirely processed by the Chemstation software from Agilent. Concentrations are calculated with a software developed at LSCE using peak height or area depending on the species.

2.2.3 Uncertainty of flask measurements

Uncertainties in the measured concentrations stemmed from both the sampling method and the analysis. Collecting flask samples in pairs and measuring each flask twice allow us to evaluate these uncertainties. A large discrepancy between two analyses of the same flask reveals a problem in the analysis system, while a difference between a pair of flasks reflects both analysis and sampling uncertainties. Flask pairs with differences in mole fractions beyond a certain threshold are flagged and rejected (see Table S2 in the Supplement for the threshold for each species). The percentages of flask pairs retained for analyses are 65.9–88.3 % for CO_2, 88.6–94.1 % for CH_4, 74.6–91.5 % for N_2O, 92.0–96.8 % for SF_6, 75.7–91.5 % for CO, and 76.2–95.2 % for H_2 (Table S3). For each species, we evaluate the uncertainties by averaging differences between the two injections of the same flask (analysis uncertainty) and between the pair of flasks (analysis uncertainty + sampling uncertainty) across all retained flask pairs from the three Indian stations (Table S4). For all species except SF_6, the sampling uncertainty turns out to be the major uncertainty, while the analysis uncertainty is equivalent to the reproducibility of the instrument. For SF_6, both uncertainties are extremely low due to the small amplitudes and variations of the signals at the three stations.

At LSCE, there are regular comparison exercises in which flasks are measured by different laboratories on the same primary scale (e.g., Inter-Comparison Project (ICP) loop, Integrated non-CO_2 Greenhouse gas Observing System (InGOS) "Cucumber" intercomparison project). These comparisons allow us to estimate possible biases in our measurements. In Table S4, the bias for each species is calculated over the sampling period using the ICP flask exercise that circulates flasks of low, medium and high concentrations between different laboratories. For CO_2, CH_4, SF_6 and CO, the biases are reported against NOAA (NOAA-LSCE) as it is the laboratory responsible for the primary scales of these species. The bias of H_2 is calculated against Max Planck Institute for Biogeochemistry (MPI-BGC) in Jena, Germany, which is responsible for the primary scale of H_2. The bias of N_2O is reported against MPI-BGC instead of NOAA. Although NOAA is responsible for the primary scale of N_2O, the instruments they use for the N_2O flask analyses and cylinder calibration are not the same as ours. For CH_4, N_2O, SF_6 and H_2, the estimated biases are within the noise level of the instrument and negligible. For CO_2 and CO, we observe a bias of -0.15 ± 0.11 ppm and 3.5 ± 2.2 ppb, respectively (Table S4), which could be due to the nonlinearity of the instrument and/or an improper attribution of the secondary scale values.

2.3 Data analyses

2.3.1 Curve-fitting procedures

For each time series of flask measurements, we calculated annual means and seasonal cycles using a curve-fitting routine (CCGvu) developed by NOAA/CMDL (Thoning et al., 1989). A smoothed function was fitted to the retained data, consisting of a first-order polynomial for the growth rate and two harmonics for the annual cycle (Levin et al., 2002; Ramonet et al., 2002), as well as a low-pass filter with 80 and 667 days as short-term and long-term cutoff values, respectively (Bakwin et al., 1998). Residuals were then calculated as the differences between the original data and the smoothed fitting curve. Any data lying outside three standard deviations of the residuals were regarded as outliers and discarded from the time series (Harris et al., 2000; Zhang et al., 2007). This procedure was repeated until no outliers remained. These outliers were likely a result of pollution by local emissions and not representative of regional background concentrations. The data discarded through this filtering procedure account for less than 4 % of the retained flask pairs after flagging (Table S3). Particularly for PON, where obser-

vations can be influenced by local emissions, we also tried to use CO as a tracer and filtered time series of other species by CO outliers. Results show that this additional filtering does not make a significant difference to the trends, seasonal cycles and mean annual gradients (relative to HLE) for all the other species at PON (Table S5, Fig. S2). On the other hand, however, the approach may substantially decrease the number of samples used to fit the smooth curve (e.g., $\sim 38\,\%$ for CH_4) and result in larger data gaps (Table S5, Fig. S2), probably compromising reliability of the analyses. Therefore, finally, we did not use CO as a tracer of local emissions for additional filtering.

For each species at each station, the annual means, as well as the amplitude and phases of seasonal cycles, were determined from the smoothed fitting curve and its harmonic component. We bootstrapped the curve-fitting procedures 1000 times by randomly sampling the original data with replacement to further estimate uncertainties of annual means and seasonal cycles. Since the observation records are relatively short, we used all flask measurements between 2006 and 2011 to fit the smooth curve when available (Fig. S3). For each species, we also compared results with measurements from stations outside India that belong to networks of NOAA/ESRL (http://www.esrl.noaa.gov/gmd/) and Integrated Carbon Observation System (ICOS, https://www.icos-cp.eu/). Locations and the fitting periods of these stations are also given in Table S6, Figs. S1 and S3.

2.3.2 Ratio of species

We analyzed CH_4–CO, CH_4–CO_2, and CO–CO_2 correlations using the residuals from the smoothed fitting curves that represent synoptic-scale variations (Harris et al., 2000; Ramonet et al., 2002; Grant et al., 2010). To determine the ratio between each species pair, as in previous studies, we used the slope calculated from the orthogonal distance regression (Press et al., 2007) to equally account for variances of both species (Harris et al., 2000; Ramonet et al., 2002; Schuck et al., 2010; Baker et al., 2012). We also bootstrapped the orthogonal distance regression procedure 1000 times and estimated the 1σ uncertainty for each ratio. The analyses were performed with R3.1.0 (R Core Team, 2014) following the procedure described in Teetor (2011).

3 Results and discussions

3.1 Annual means and seasonal cycles

3.1.1 CO_2

Figure 2 shows CO_2 flask measurements and the corresponding smooth curves fitted to the data at HLE, PON and PBL, as well as two additional NOAA/ESRL stations, namely the Assy Plateau, Kazakhstan (KZM – 43.25° N, 77.88° E, 2519 m a.s.l.) and Mt. Waliguan, China (WLG – 36.29 ° N, 100.90 ° E, 3810 m a.s.l.) (Dlugokencky et al., 2014b). HLE observed an increase in CO_2 mole fractions from 382.3 ± 0.3 to 391.4 ± 0.3 between 2007 and 2011, with annual mean values being lower (by 0.2–1.9 ppm) than KZM and WLG (Fig. 2c and d, Table 1). At PON, the annual mean CO_2 mole fractions were generally higher than at HLE, with differences ranging 1.8–4.3 ppm (Fig. 2a, Table 1). The annual mean CO_2 gradient between PON and HLE reflects the altitudinal difference of the two stations, and a larger influence of CO_2 emissions at PON, mostly from southern India (Fig. 1a, EDGAR v4.2, 2011). Additionally, as shown in Fig. 2a and Table 1, the CO_2 observations at PON are influenced by synoptic scale events, with a large variability of individual measurements relative to the fitting curve (see the relative SDs (RSDs) in Table 1). At PBL, the annual mean CO_2 mole fractions were on average 1.2–1.8 ppm lower than that at HLE (Table 1). The negative gradient between PBL and HLE is particularly large during summer, possibly due to clean air masses transported from the ocean (Figs. 1a and 2b). Note that caution should be exercised in interpreting the gradient at PBL because of the data gap and short duration of the time series.

The different CO_2 seasonal cycles observed at the five stations reflect the seasonality of carbon exchange in the northern terrestrial biosphere as well as influences of long-range transport and the monsoon circulations. At HLE, the peak-to-peak amplitude of the mean seasonal cycle was 8.2 ± 0.4 ppm, with the maximum early May and the minimum mid-September, respectively (Fig. 3, Table 1). The mean seasonal cycle estimated from flask measurements at HLE is in good agreement with that derived from vertical profiles of in situ aircraft measurements over New Delhi (~ 500 km southwest of HLE) from the Comprehensive Observation Network for Trace gases by Airliner (CONTRAIL, http://www.cger.nies.go.jp/contrail/) project at similar altitudes ($R = 0.98$–0.99, $p < 0.001$, Fig. 3a; Machida et al., 2008), and back trajectories show that they represent air masses with similar origins as HLE (Fig. S8), confirming that HLE is representative of the regional free mid-troposphere background concentrations. When comparing with the two other background stations located further north in Central and East Asia, a significant delay of the CO_2 phase is seen at HLE compared to KZM and WLG (Fig. 3b, Table 1). We also note that the CO_2 mean seasonal cycle at HLE is in phase with the composite zonal marine boundary layer (MBL) reference at 32° N, while for KZM and WLG, an advance in the CO_2 phase by about 1 month is observed compared to the zonal MBL reference (Fig. S4; Dlugokencky et al., 2014b). The phase shifts in the CO_2 seasonal cycles mainly result from differences in the air mass origins between stations. HLE is influenced by the long-range transport of air masses from mid-latitudes around 30° N, as well as air masses passing over the Indian subcontinent in the boreal summer (Fig. 1a); therefore, its CO_2 seasonal cycle is related to the seasonality of vegetation activity over the en-

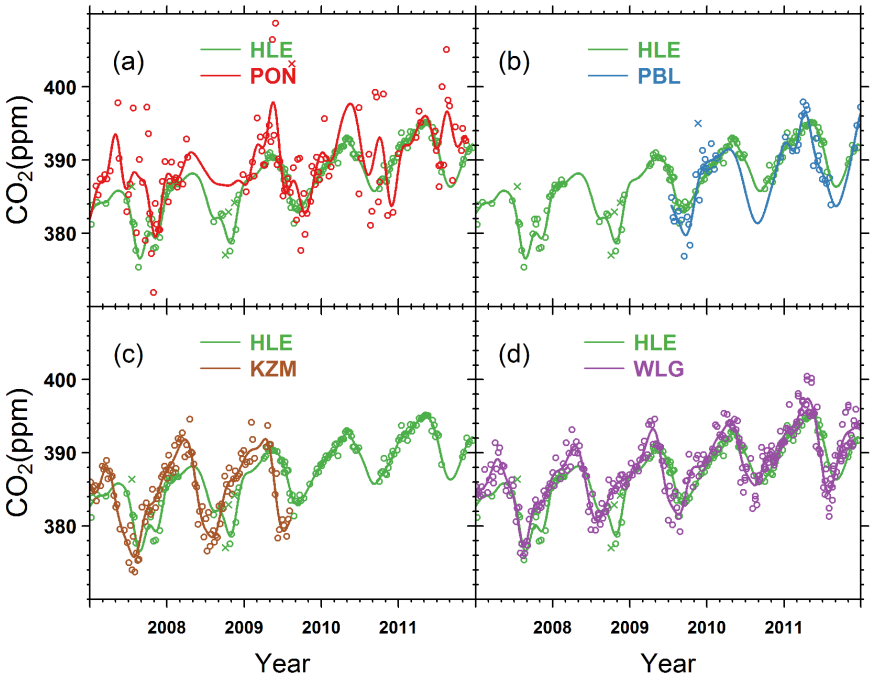

Figure 2. Time series of CO_2 flask measurements at **(a)** HLE and PON, **(b)** HLE and PBL, **(c)** HLE and KZM, and **(d)** HLE and WLG. The open circles denote flask data used to fit the smoothed curves, while the crosses denote discarded flask data lying outside 3 times the residual standard deviations from the smoothed curve fits. For each station, the smoothed curve is fitted using Thoning's method (Thoning et al., 1989) after removing outliers.

tire latitude band. KZM and WLG receive air masses passing over the Middle East and western Asia as HLE does, but they are also influenced by air masses of more northern origins with signals of strong CO_2 uptake over Siberia during JAS (Fig. S5). At WLG, negative CO_2 synoptic events, indicative of large-scale transport of air masses exposed to carbon sinks in Siberia in summer, were also detected by in situ measurements during 2009–2011 (Fang et al., 2014). Moreover, the back trajectories indicate that WLG and KZM are more influenced than HLE by air masses that have exchanged with the boundary layer air being affected by vegetation CO_2 uptake (Fig. S6a, d, e). This could additionally account for the earlier CO_2 phase observed at KZM and WLG compared to HLE.

At PON and PBL, the peak-to-peak amplitudes of the CO_2 mean seasonal cycles were 7.6 ± 1.4 and 11.1 ± 1.3 ppm, with their maxima observed in April. The CO_2 mean seasonal cycle is controlled by changes in the monsoon circulations, in combination with the seasonality of CO_2 biotic exchange and anthropogenic emissions in India. During the boreal winter when the NE monsoon prevails, PON and PBL receive air masses enriched in CO_2 from the eastern and northeastern Indian subcontinent as well as from Southeast Asia, with large anthropogenic CO_2 emissions (EDGAR v4.2, 2011; Wang et al., 2013; Kurokawa et al., 2013). During April when the SW monsoon begins to develop, the two stations record a decrease in CO_2 because of the arrival of air masses depleted in CO_2 originating from the Indian Ocean south of the Equator (Figs. 1a, 3c). Compared to PBL, the CO_2 decrease at PON is less pronounced and longer, probably because of the influence of anthropogenic emissions in southern India. The CO_2 mean seasonal cycle at PON is also similar to that observed at CRI (15.08° N, 73.83° E, 60 m a.s.l.), another station on the southwest coast of India, yet the seasonal maximum at CRI is reached slightly earlier than at PON in March (Bhattacharya et al., 2009; Tiwari et al., 2011, 2014). The SNG station (18.35° N, 73.75° E, 1600 m a.s.l.), located in the Western Ghats, observes a larger CO_2 seasonal cycle with a peak-to-peak amplitude of ~ 20 ppm (Tiwari et al., 2014).

3.1.2 CH_4

Figure 4 presents the time series of CH_4 flask measurements at the three Indian stations and the two NOAA/ESRL stations (Dlugokencky et al., 2014a), with their corresponding smoothed curves for 2007–2011. At HLE, the annual mean CH_4 concentration increased from 1814.8 ± 2.9 to 1849.5 ± 5.2 ppb between 2007 and 2011 (Fig. 4, Table 1). The multiyear mean CH_4 value at HLE was lower than at KZM and WLG by on average 25.7 ± 3.1 and 19.6 ± 7.8 ppb (Fig. 4c and d, Table 1), respectively, reflecting the latitudinal and altitudinal CH_4 gradients. Indeed, KZM and WLG receive air masses transported from Siberia with large wetland

Table 1. Annual mean values, trends, and average peak-to-peak amplitudes of trace gases at HLE, PON, PBL and the two additional NOAA/ESRL stations – KZM and WLG. For each species at each station, the annual mean values and average peak-to-peak amplitude are calculated from the smoothed curve and mean seasonal cycle, respectively. The residual standard deviation (RSD) around the smoothed curve and the Julian days corresponding to the maximum (D_{max}) and minimum (D_{min}) of the mean seasonal cycle are given as well. Uncertainty of each estimate is calculated from 1 SD of 1000 bootstrap replicates. At PON, PBL and KZM, annual mean values and/or trends may not be applicable (n/a) due to data gaps.

	HLE	PON	PBL	KZM	WLG
CO_2 (ppm)					
Annual mean 2007	382.3 ± 0.3	386.6 ± 0.9	n/a	382.7 ± 0.2	384.2 ± 0.2
Annual mean 2008	384.6 ± 0.5	388.1 ± 0.9	n/a	385.7 ± 0.2	386.0 ± 0.2
Annual mean 2009	387.2 ± 0.2	389.0 ± 0.6	n/a	n/a	387.4 ± 0.2
Annual mean 2010	389.4 ± 0.1	391.3 ± 1.5	387.6 ± 0.7	n/a	390.1 ± 0.2
Annual mean 2011	391.4 ± 0.3	n/a	390.2 ± 0.6	n/a	392.2 ± 0.2
Trend (yr^{-1})	2.1 ± 0.0	1.7 ± 0.1	n/a	n/a	2.0 ± 0.0
(Trend at MLO: 2.0 ± 0.0)					
RSD	0.7	4.0	1.5	1.5	1.4
Amplitude	8.2 ± 0.4	7.6 ± 1.4	11.1 ± 1.3	13.8 ± 0.5	11.1 ± 0.4
D_{max}	122.0 ± 2.9	111.0 ± 13.4	97.0 ± 26.0	75.0 ± 2.6	100.0 ± 1.5
D_{min}	261.0 ± 3.0	327.0 ± 54.3	242.0 ± 7.7	205.0 ± 2.1	222.0 ± 1.6
CH_4 (ppb)					
Annual mean 2007	1814.8 ± 2.9	1859.2 ± 6.7	n/a	1842.6 ± 2.4	1841.0 ± 1.8
Annual mean 2008	1833.1 ± 5.4	1856.1 ± 10.4	n/a	1856.6 ± 2.3	1845.6 ± 1.5
Annual mean 2009	1830.2 ± 1.7	1865.7 ± 5.1	n/a	n/a	1851.8 ± 1.9
Annual mean 2010	1830.5 ± 2.1	1876.9 ± 9.1	1867.5 ± 15.4	n/a	1857.6 ± 1.4
Annual mean 2011	1849.5 ± 5.2	n/a	1852.0 ± 7.6	n/a	1859.9 ± 1.2
Trend (yr^{-1})	4.9 ± 0.0	9.4 ± 0.1	n/a	n/a	5.3 ± 0.0
(Trend at MLO: 6.2 ± 0.0)					
RSD	9.1	34.4	22.4	14.6	12.3
Amplitude	28.9 ± 4.2	124.1 ± 10.2	143.9 ± 12.4	22.7 ± 4.7	17.5 ± 2.2
D_{max}	219.0 ± 4.6	337.0 ± 6.1	345.0 ± 87.6	236.0 ± 43.2	222.0 ± 6.2
D_{min}	97.0 ± 58.9	189.0 ± 10.7	193.0 ± 13.5	338.0 ± 39.0	340.0 ± 96.6
N_2O (ppb)					
Annual mean 2007	322.2 ± 0.1	324.8 ± 0.3	n/a		
Annual mean 2008	322.9 ± 0.1	326.3 ± 0.3	n/a		
Annual mean 2009	323.5 ± 0.1	326.7 ± 0.3	n/a		
Annual mean 2010	324.0 ± 0.1	327.1 ± 0.5	329.0 ± 0.5		
Annual mean 2011	325.2 ± 0.1	n/a	327.9 ± 0.3		
Trend (yr^{-1})	0.8 ± 0.0	0.8 ± 0.1	n/a		
(Trend at MLO: 1.0 ± 0.0)					
RSD	0.3	1.4	1.1		
Amplitude	0.6 ± 0.1	1.2 ± 0.5	2.2 ± 0.6		
D_{max}	227.0 ± 11.8	262.0 ± 83.2	313.0 ± 42.6		
D_{min}	115.0 ± 16.4	141.0 ± 48.2	65.0 ± 33.4		
SF_6 (ppt)					
Annual mean 2007	6.26 ± 0.03	6.19 ± 0.01	n/a		
Annual mean 2008	6.54 ± 0.03	6.49 ± 0.02	n/a		
Annual mean 2009	6.79 ± 0.01	6.77 ± 0.01	n/a		
Annual mean 2010	7.17 ± 0.01	7.08 ± 0.02	7.10 ± 0.07		
Annual mean 2011	7.38 ± 0.01	n/a	7.45 ± 0.03		
Trend (yr^{-1})	0.29 ± 0.05	0.31 ± 0.05	n/a		
(Trend at MLO: 0.29 ± 0.03)					

Table 1. Continued.

	HLE	PON	PBL	KZM	WLG
RSD	0.07	0.05	0.12		
Amplitude	0.15 ± 0.03	0.24 ± 0.02	0.48 ± 0.07		
D_{max}	320.0 ± 8.3	327.0 ± 12.1	342.0 ± 59.9		
D_{min}	211.0 ± 65.1	204.0 ± 3.3	210.0 ± 18.1		
CO (ppb)					
Annual mean 2007	104.7 ± 1.4	200.5 ± 7.8	n/a	121.7 ± 1.7	141.0 ± 4.3
Annual mean 2008	103.1 ± 2.1	175.3 ± 13.1	n/a	123.7 ± 1.7	129.0 ± 2.9
Annual mean 2009	98.9 ± 1.9	174.3 ± 4.8	n/a	n/a	131.9 ± 3.7
Annual mean 2010	99.0 ± 1.2	185.1 ± 8.7	157.6 ± 20.4	n/a	130.2 ± 3.9
Annual mean 2011	99.4 ± 2.2	n/a	145.9 ± 9.9	n/a	124.0 ± 2.3
Trend (yr^{-1})	-2.2 ± 0.0	0.4 ± 0.1	n/a	n/a	-1.9 ± 0.0
(Trend at MLO: -1.6 ± 0.0)					
RSD	6.5	32.0	30.8	11.8	22.5
Amplitude	28.4 ± 2.3	78.2 ± 11.6	144.1 ± 16.0	37.1 ± 4.4	38.6 ± 5.1
D_{max}	79.0 ± 11.4	4.0 ± 160.2	12.0 ± 117.9	72.0 ± 5.0	94.0 ± 38.2
D_{min}	297.0 ± 5.3	238.0 ± 46.1	213.0 ± 23.0	318.0 ± 6.1	331.0 ± 6.2
H_2 (ppb)					
Annual mean 2007	539.6 ± 2.1	574.5 ± 2.4	n/a	502.4 ± 2.0	500.9 ± 1.5
Annual mean 2008	533.2 ± 3.2	558.2 ± 5.3	n/a	n/a	n/a
Annual mean 2009	533.3 ± 1.6	562.4 ± 1.6	n/a	n/a	n/a
Annual mean 2010	533.5 ± 1.8	563.9 ± 2.3	558.6 ± 2.4	n/a	n/a
Annual mean 2011	536.9 ± 1.5	n/a	555.4 ± 1.6	n/a	n/a
Trend (yr^{-1})	-0.5 ± 0.0	-1.3 ± 0.1	n/a	n/a	n/a
RSD	6.6	8.4	7.0	13.3	9.5
Amplitude	15.8 ± 2.2	21.6 ± 3.4	21.3 ± 5.0	16.7 ± 4.0	22.8 ± 3.0
D_{max}	120.0 ± 8.7	96.0 ± 9.6	99.0 ± 8.8	120.0 ± 34.2	51.0 ± 13.4
D_{min}	266.0 ± 39.6	219.0 ± 10.3	353.0 ± 87.8	341.0 ± 78.3	298.0 ± 6.5

CH_4 emissions in summer, as well as those from regional sources closer to the stations (Fang et al., 2013; Fig. S5), which may further contribute to the positive gradients between these two stations and HLE. At PON and PBL, the annual mean CH_4 mole fractions were higher than those at HLE by as much as 37.4 ± 10.7 and 19.8 ± 24.5 ppb respectively (Fig. 4a and b, Table 1). The positive gradients indicate significant regional CH_4 emissions, especially during winter when the NE monsoon transports air masses from eastern and northeastern India and Southeast Asia, where emissions from livestock, rice paddies and a variety of waterlogged anaerobic sources and residential biofuel burning are high (EDGAR v4.2, 2011; Baker et al., 2012; Kurokawa et al., 2013). The in situ measurements at Darjeeling, India (27.03° N, 88.25° E, 2194 m a.s.l.), another station located in the eastern Himalayas, also showed large variability and frequent pollution events in CH_4 mole fractions, which largely result from the transport of CH_4-polluted air masses from the densely populated Indo-Gangetic Plain to the station (Ganesan et al., 2013).

The CH_4 seasonal cycles exhibit contrasting patterns across stations. As shown in Fig. 5, a distinct characteristic of the mean seasonal cycle at HLE is a CH_4 maximum from June to September. Even KZM and WLG do not show a minimum in summer that would be characteristic for the enhanced CH_4 removal rate by reaction with OH. The pronounced HLE feature is consistent with the result from the aircraft flask measurements over India at flight altitudes of 8–12.5 km by the Civil Aircraft for the Regular Investigation of the atmosphere Based on an Instrument Container (CARIBIC, http://www.caribic-atmospheric.com/) project (Schuck et al., 2010, 2012; Baker et al., 2012), although a larger seasonal cycle amplitude is found in the CARIBIC composite data due to the rapid vertical mixing over the monsoon region and the strong anticyclone that develops in the upper troposphere (Fig. 5a; Schuck et al., 2010). CARIBIC sampled the mid-to-upper tropospheric air masses that were earlier and more strongly enriched in CH_4, as a result of the rapid vertical transport of surface air masses by deep convection and subsequent accumulation and confinement of pollutants within the strong, closed circulation of the anticyclone (Li et al., 2005; Randel and Park, 2006). Xiong et al. (2009) also reported enhancements of CH_4 during the summer monsoon season over South Asia based on satellite

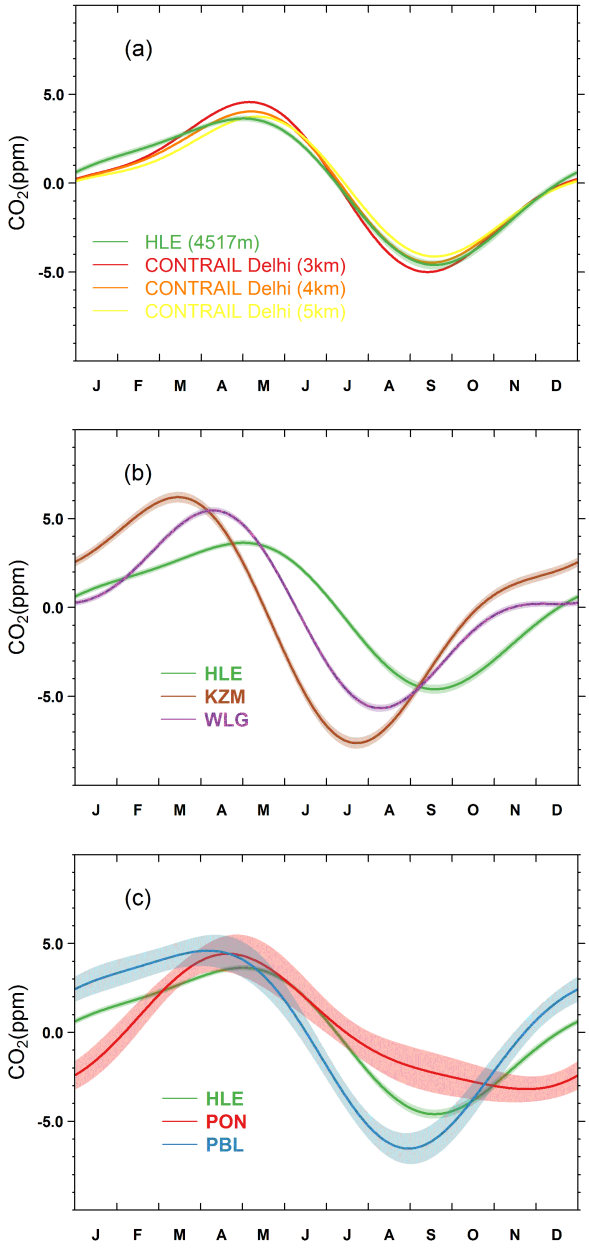

Figure 3. (a) The mean CO_2 seasonal cycle at HLE, in comparison with the mean seasonal cycles derived from the in situ CO_2 measurements over New Delhi at different altitude bands (3–4, 4–5, and 5–6 km) by the CONTRAIL project (2006–2010). **(b)** The mean CO_2 seasonal cycles at HLE, KZM and WLG. **(c)** The mean CO_2 seasonal cycles at HLE, PON and PBL. For each station, the mean seasonal cycle is derived from the harmonics of the smoothed fitting curve in Fig. 2. Shaded area indicates the uncertainty of the mean seasonal cycle calculated from 1 SD of 1000 bootstrap replicates. For the CONTRAIL data sets, CO_2 measurements over New Delhi were first averaged by altitude bands. A fitting procedure was then applied to the aggregated CO_2 measurements to generate the mean season cycle for different altitude bands.

retrievals of CH_4 using the Atmospheric Infrared Sounder (AIRS) on the EOS/Aqua platform as well as model simulations. Moreover, the mean CH_4 seasonal cycle at HLE agrees well with the seasonal variations of CH_4 emissions from wetlands and rice paddies and convective precipitation over the Indian subcontinent (Fig. 5b), suggesting that the summer maximum at HLE is likely related to the enhanced biogenic CH_4 emissions from wetlands and rice paddies and deep convection that mixes surface emissions into the mid-to-upper troposphere. During the SW monsoon period (June–September), convection over the Indian subcontinent and the Bay of Bengal rapidly mixes surface-polluted air with the upper troposphere, therefore concentrations of trace gases would be enhanced at higher altitudes rather than at the surface (Schuck et al., 2010; Lawrence and Lelieveld, 2010). Further analyses of carbon isotopic measurements and/or chemical transport model are needed to disentangle and quantify the contributions of meteorology and biogenic emissions to the CH_4 summer maximum at HLE. As stated above, KZM and WLG also record CH_4 increases during summertime, but with smaller magnitudes (Fig. 5a), possibly because they are not directly influenced by deep convection from the Indian monsoon system.

In contrast to HLE, the CH_4 mean seasonal cycles at PON and PBL have distinct phases and much larger amplitudes, with minimum CH_4 values during July (Fig. 5c). These not only reflect higher rates of removal by OH, but also the influence of southern hemispheric air transported at low altitudes from the southwest as well as the dilution effect from the increased local planetary boundary layer height. In boreal winter, the maxima at PON and PBL are associated with CH_4-enriched air masses transported from eastern and northeastern India, and Southeast Asia, mostly polluted by agricultural-related sources (e.g., livestock, rice paddies, agricultural waste burning). As PON and PBL, the flask measurements at CRI also showed the seasonal maximum CH_4 values during the NE monsoon season, reflecting influences of air masses with elevated CH_4 from the Indian subcontinent (Bhattacharya et al., 2009; Tiwari et al., 2013).

3.1.3 N_2O

Nitrous oxide (N_2O) is a potent greenhouse gas that has the third largest contribution to anthropogenic radiative forcing after CO_2 and CH_4 (IPCC, 2013). It has also become the dominant ozone-depleting substance (ODS) emitted in the 21st century with the decline of chlorofluorocarbons (CFCs) under the Montreal Protocol (Ravishankara et al., 2009). Since the pre-industrial era, atmospheric N_2O has increased rapidly from $\sim$270 to $\sim$325 ppb in 2011 (IPCC, 2013), largely as the result of human activities. Of the several known N_2O sources, agricultural activities (mainly through nitrogen fertilizer use) are responsible for $\sim$58 % of the global anthropogenic N_2O emissions, with a higher share in a pre-

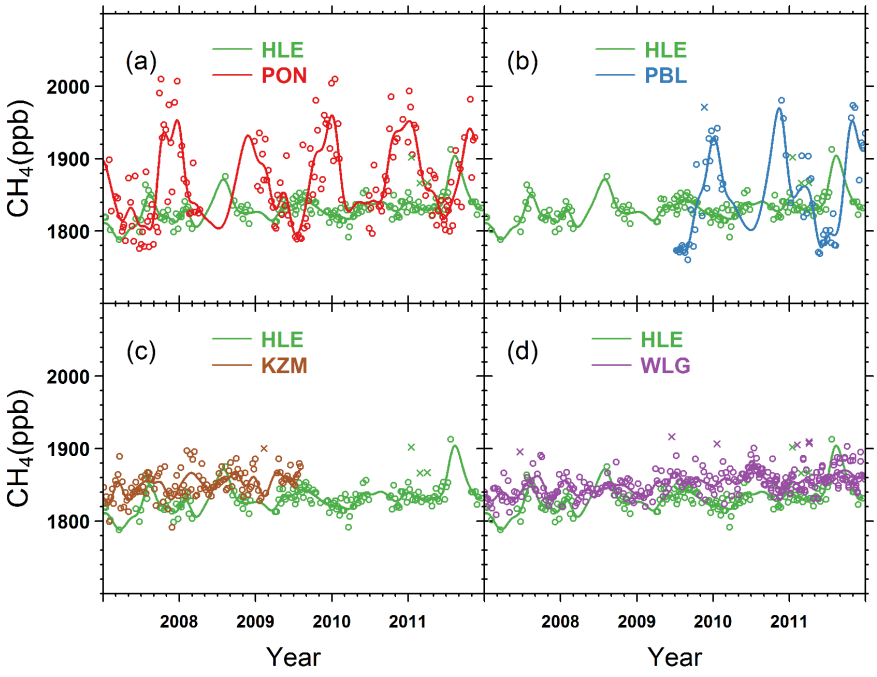

Figure 4. Time series of CH_4 flask measurements at **(a)** HLE and PON, **(b)** HLE and PBL, **(c)** HLE and KZM, and **(d)** HLE and WLG. The open circles denote flask data used to fit the smoothed curves, while the crosses denote discarded flask data lying outside 3 times the residual standard deviations from the smoothed curve fits. For each station, the smoothed curve is fitted using Thoning's method (Thoning et al., 1989) after removing outliers.

dominantly agrarian country like India (∼ 75 %; Garg et al., 2012).

The time series of N_2O flask measurements over the period of 2007–2011 and their smoothed curves are presented in Fig. 6. At HLE, the annual mean N_2O concentration rose from 322.2 ± 0.1 to 325.2 ± 0.1 ppb during 2007–2011 (Table 1), with a mean annual growth rate of 0.8 ± 0.0 ppb yr^{-1} ($r^2 = 0.97$, $p = 0.001$), smaller than that at MLO (1.0 ± 0.0 ppb yr^{-1}, Table 1). At PON and PBL, the annual mean N_2O mole fractions are higher than at HLE by 3.1 ± 0.3 and 3.8 ± 1.7 ppb (Fig. 6, Table 1), respectively. The N_2O gradients between PON, PBL and HLE are larger than typical N_2O gradients observed between stations scattered in Europe or in North America. For example, Haszpra et al. (2008) presented N_2O flask measurements at a continental station – Hegyhátsál, Hungary (HUN – 46.95 ° N, 16.65° W, 248 m a.s.l.), from 1997 to 2007. The annual mean N_2O mole fraction at HUN was higher than at Mace Head (MHD) by only 1.3 ppb. We also analyzed N_2O time series of flask measurements during 2007–2011 at several European coastal stations – BGU in Spain, FIK in Greece, and LPO in France (Table S6), and the N_2O gradients between these stations and MHD were 1.1 ± 0.2, 0.4 ± 0.1, and 2.1 ± 0.6 ppb, respectively (Fig. S10, Table S7). In the United States, N_2O flask measurements from the NOAA/ESRL stations at Park Falls, Wisconsin (LEF – 45.95° N, 90.27° W, 472 m a.s.l.), Harvard Forest, Massachusetts (HFM – 42.54° N, 72.17° W, 340 m a.s.l.), and a continental, high-altitude station at Niwot Ridge, Colorado (NWR – 40.05° N, 105.58° W, 3523 m a.s.l.), also show that the annual mean N_2O concentrations at HFM and LEF were higher than that at NWR by only 0.5 ± 0.1 and 0.3 ± 0.1 ppb, respectively (Fig. S10, Table S7). Additionally, the N_2O concentrations measured at PON and PBL have a notably higher variability (around the smoothed fitting curve) than that at European and US stations (see relative SDs (RSDs) in Tables 1 and S7). The larger N_2O gradient between PON, PBL and HLE, as well as higher variability at PON and PBL, demonstrate the presence of substantial N_2O sources in South Asia and over the Indian Ocean during the observation period. The in situ measurements at Darjeeling also exhibited N_2O enhancements to be above the background level, suggesting significant N_2O sources in this region (Ganesan et al., 2013). These sources may be related to emissions from natural and cultivated soils probably enhanced by extensive use of nitrogen fertilizers, as well as emissions from regions of coastal upwelling in the Arabian Sea (Bange et al., 2001; Garg et al., 2012; Saikawa et al., 2014).

Compared to CO_2 and CH_4, the seasonal cycle of N_2O is very small due to the long lifetime of ∼ 120 years (Minschwaner et al., 1993; Volk et al., 1997), and has a larger uncertainty probably because synoptic events are more likely to mask the seasonal signal. At HLE, PON and PBL, the peak-to-peak amplitudes of the N_2O seasonal cycle are 0.6 ± 0.1,

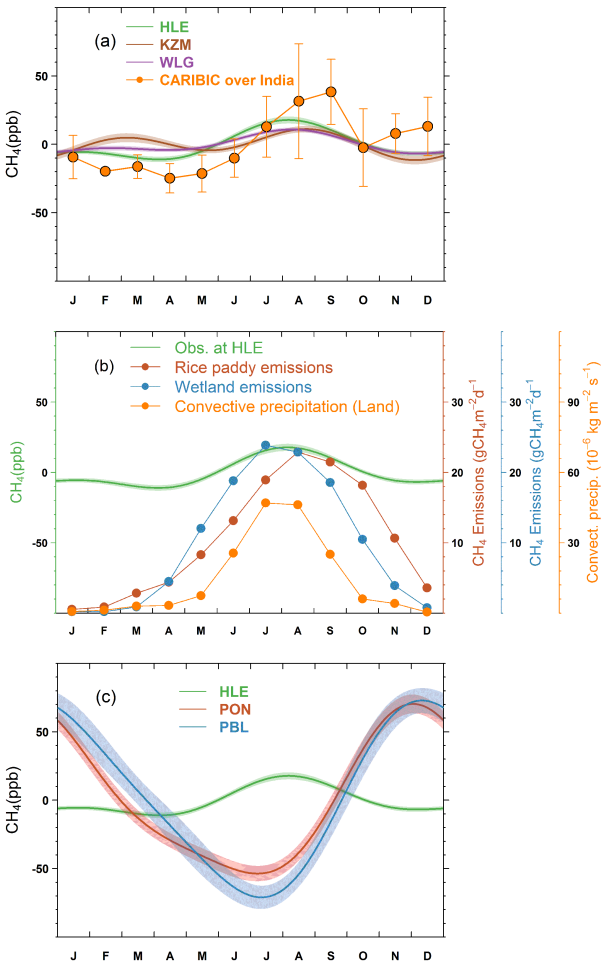

Figure 5. (a) The mean CH_4 seasonal cycles observed at HLE, KZM and WLG. The mean CH_4 seasonal cycle derived from aircraft flask measurements by the CARIBIC project is also presented. The CARIBIC flask measurements in the upper troposphere (200–300 hPa) during 2005–2012 are averaged over the Indian subcontinent (10–35° N, 60–100° E) by month to generate the mean seasonal cycle. The error bars indicate 1 standard deviation of CH_4 flask measurements within the month. **(b)** The seasonal variations of CH_4 emissions from rice paddies and wetlands over the Indian subcontinent. The CH_4 emissions from rice paddies are extracted from a global emission map for the year 2010 (EDGAR v4.2, 2011), imposed by the seasonal variation on the basis of Matthews et al. (1991). The CH_4 emissions from wetlands are extracted from outputs of a global vegetation model (BIOME4-TG, Kaplan et al., 2006). The seasonal variation of deep convection over the Indian subcontinent is also presented, indicated by convective precipitation obtained from an LMDZ simulation nudged with ECMWF reanalysis (Hauglustaine et al., 2004). The CH_4 emissions and convective precipitation are averaged over the domain 10–35° N, 70–90° E to give a regional mean estimate. **(c)** The mean CH_4 seasonal cycles observed at HLE, PON and PBL. For each station, the mean seasonal cycle is derived from the harmonics of the smoothed fitting curve in Fig. 4. Shaded area indicates the uncertainty of the mean seasonal cycle calculated from 1 SD of 1000 bootstrap replicates.

1.2 ± 0.5, and 2.2 ± 0.6 ppb, respectively (Table 1). HLE displays a N_2O maximum in mid-August (Student's t test, $t = 1.78$, $p = 0.06$), and a secondary maximum is in January/February but not significant (Student's t test, $t = -0.84$, $p = 0.79$) (Table 1, Fig. 7, Table S8 for detailed t test statistics). The N_2O seasonal cycle at HLE is out of phase with that at other northern background stations such as MHD (Fig. S11, Table S7), where an N_2O summer minimum is always observed, likely due to the downward transport of N_2O-depleted air from the stratosphere to the troposphere during spring and summer (Liao et al., 2004; Morgan et al., 2004; Jiang et al., 2007b). The timing of the summer N_2O maximum at HLE is consistent with that of CH_4 (Table 1; Figs. 5 and 7), giving evidence that the N_2O seasonal cycle is probably influenced by the convective mixing of surface air, rather than by the influx of stratospheric air into the troposphere. Given that the populous Indo-Gangetic Plain has high N_2O emission rates due to the intensive use of nitrogen fertilizers (Garg et al., 2012; Thompson et al., 2014a), during summer, the surface air enriched in N_2O is vertically transported by deep convection and enhances N_2O mole fractions in the mid-to-upper troposphere. Like CH_4, the N_2O enhancement during the summer monsoon period (June–September) was also observed by the aircraft flask measurements at flight altitudes 8–12.5 km from the CARIBIC project in 2008 (Schuck et al., 2010).

At PON, N_2O also decreases during February–April and reaches a minimum at the end of May. However, the decrease of N_2O does not persist during June–September, which is in contrast with CH_4 (Table 1, Fig. 7a). One reason may be that the air masses arriving at the site during the southwest monsoon period is relatively enriched in N_2O compared to CH_4, reflecting differences in their relative emissions along the air mass route. The increase of N_2O at PON during June–August and the maximum during September–October are likely related to N_2O emissions from coastal upwelling along the southern Indian continental shelf, which peak during the SW monsoon season (Patra et al., 1999; Bange et al., 2001). According to Bange et al. (2001), the annual N_2O emissions for the Arabian Sea are 0.33–0.70 Tg yr^{-1}, of which N_2O emissions during the SW monsoon account for about 64–70 %. This coastal upwelling N_2O flux is significantly larger than the annual anthropogenic N_2O emissions in southern India south of 15° N, which is estimated to be on average 0.07–0.08 Tg yr^{-1} during 2000–2010 (EDGAR v4.2, 2011). At PBL, the maximum and minimum N_2O occur in November and February/March, respectively (Table 1, Fig. 7b). The late N_2O peak at PBL in November might be associated with the N_2O-enriched air masses transported from South and Southeast Asia, which could be attributed to natural and agricultural N_2O emissions from this region (Saikawa et al., 2014). It should be noted that the mean seasonal cycles of N_2O at PON and PBL are subject to high uncertainties because of the short observation periods and data gaps (shaded area in Fig. 7). The N_2O maximum and/or minimum obtained from

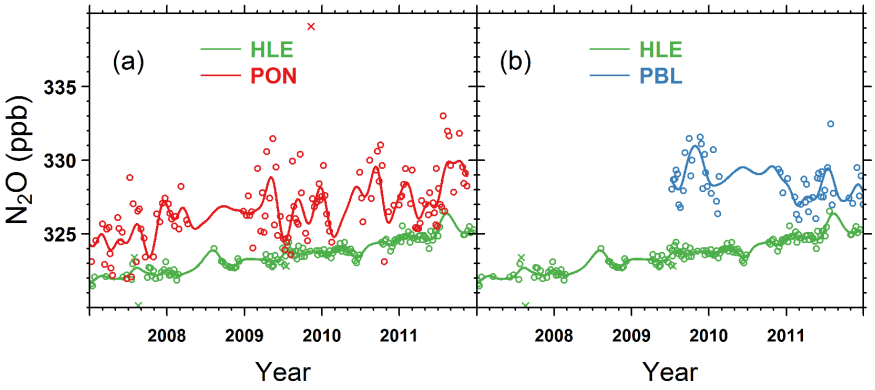

Figure 6. Time series of N_2O flask measurements at **(a)** HLE and PON and **(b)** HLE and PBL. The open circles denote flask data used to fit the smoothed curves, while crosses denote discarded flask data lying outside 3 times the residual standard deviations from the smoothed curve fits. For each station, the smoothed curve is fitted using Thoning's method (Thoning et al., 1989) after removing outliers.

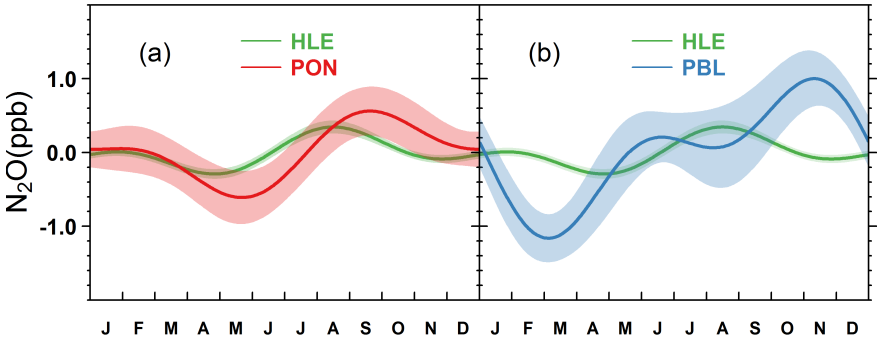

Figure 7. The mean N_2O seasonal cycles observed at **(a)** HLE and PON and **(b)** HLE and PBL. For each station, the mean seasonal cycle is derived from the harmonics of the smoothed fitting curve in Fig. 6. Shaded area indicates the uncertainty of the mean seasonal cycle calculated from 1 SD of 1000 bootstrap replicates.

the mean seasonal cycle are marginally significant for PON and PBL (Table S8 for detailed t test statistics). Therefore, caution should be exercised in interpreting mean seasonal cycles at these stations. Sustained, long-term measurements are needed in order to generate more reliable estimates of the seasonal cycles for the two stations.

3.1.4 SF_6

Sulfur hexafluoride (SF_6) is an extremely stable greenhouse gas, with an atmospheric lifetime as long as 800–3200 years and a global warming potential (GWP) of ~23 900 over a 100-year time horizon (Ravishankara et al., 1993; Morris et al., 1995; IPCC, 2013). The main sources of atmospheric SF_6 emissions are electricity distribution systems, magnesium production, and semi-conductor manufacturing (Olivier et al., 2005), while its natural sources are negligible (Busenberg and Plummer, 2000). As its sources are almost purely anthropogenic (Maiss et al., 1996), SF_6 is widely considered as a good tracer for population density, energy consumption and anthropogenic GHG emissions (Haszpra et al., 2008).

Figure 8 presents the time series of SF_6 flask measurements and corresponding fitting curves at HLE, PON, and PBL. At HLE, the annual mean SF_6 mole fractions increased from 6.26 ± 0.03 to 7.38 ± 0.01 ppt between 2007 and 2011, which is in good agreement with the SF_6 trend observed at MLO during the same period (HLE: 0.29 ± 0.05 ppt yr^{-1}, $r^2 = 0.99$, $p < 0.001$; MLO: 0.29 ± 0.03 ppt yr^{-1}, $r^2 = 0.99$, $p < 0.001$; Figs. 8 and S12a, Tables 1, S9). The annual mean SF_6 gradient between PON and HLE is -0.060 ± 0.030 ppt, whereas the gradient between PBL and HLE is statistically insignificant (-0.002 ± 0.097 ppt). The slight negative gradient between PON and HLE is a reversed signal compared with the SF_6 observations at stations influenced by continental emissions in Europe and United States. For example, the SF_6 mole fractions at HUN over the years of 1997–2007 are higher than those at MHD by on average 0.19 ppt (Haszpra et al., 2008). We also analyzed the SF_6 gradients (relative to MHD) for two European stations – BGU (41.97° N, 3.30° E, 30 m a.s.l.) and LPO (48.80° N, 3.57° W, 30 m a.s.l.), which are 0.10 ± 0.03 and 0.05 ± 0.02 ppt averaged over the period of 2007–2011, respectively. At HFM, the SF_6 mole

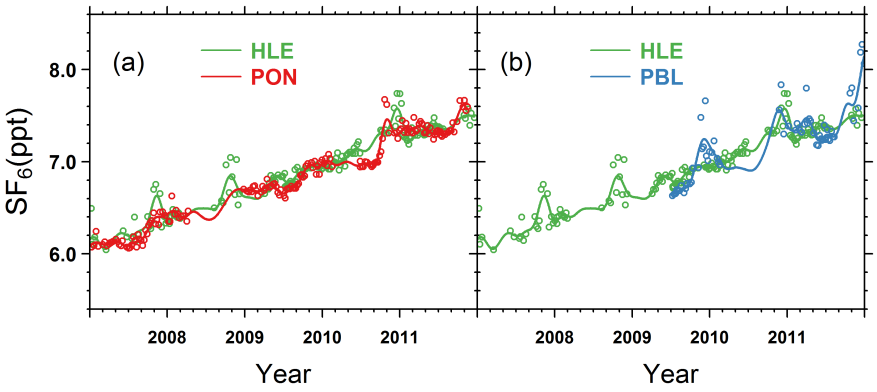

Figure 8. Time series of SF_6 flask measurements at **(a)** HLE and PON and **(b)** HLE and PBL. The open circles denote flask data used to fit the smoothed curves. For each station, the smoothed curve is fitted using Thoning's method (Thoning et al., 1989) after removing outliers.

fractions are higher than those of the NWR on average by 0.15 ± 0.06 ppt during 2007–2011 (Table S9). Given the long atmospheric lifetime of SF_6, the positive gradients between continental European and US stations and background reference stations suggest significant sources in Europe and the US. The slight negative gradient between PON and HLE implies weak SF_6 emissions over the Indian subcontinent, which is also indicated by recent high-frequency in situ SF_6 measurements at Darjeeling (Ganesan et al., 2013). It is also worthwhile to note that high SF_6 values occur repeatedly at HLE and PBL in winter, which is likely related to episodic SF_6 pollution events from the Middle East, South/Southeast Asia and China (Figs. 8b and S7d).

The annual mean SF_6 seasonal cycles for HLE, PON, and PBL are presented in Fig. 9. The peak-to-peak amplitudes at the three stations are 0.15 ± 0.03, 0.24 ± 0.02, and 0.48 ± 0.07 ppt, respectively (Table 1). At HLE, the SF_6 seasonal cycle is bimodal as for N_2O, with an absolute maximum occurring in November (Student's t test, $t = 2.425$, $p = 0.014$) and a secondary maximum in May (Student's t test, $t = 2.443$, $p = 0.016$) (Table S10 for detailed t test statistics). Given that SF_6 increases monotonously and that its sources are purely anthropogenic and not subject to seasonally variations (Maiss et al., 1996), the seasonal cycle of SF_6 should be driven by changes in atmospheric circulations, e.g., the SW monsoon convection and stratosphere–troposphere exchange (Levin et al., 2002). We note that, at HLE, no enhancement of SF_6 during the SW monsoon season is recorded, unlike what is observed for CH_4 and N_2O (Figs. 5 and 7). Although the CARIBIC aircraft flask measurements over the Indian region demonstrated SF_6 enhancements in the upper troposphere at $\sim 30°$ N (approximately where HLE is located) in August, 2008, they are not related to the deep convection and surface sources that contribute to the summer maxima in CH_4 and N_2O. Back trajectories from the CARIBIC flights showed that the summer enhancements in SF_6 were related to air samples collected north of 20° N along the flight routes, where air masses were more influenced by the westerly subtropical jet (and a smaller anticyclone embedded in it over the Arabian Peninsula) rather than the deep convection in the monsoon region (Krishnamurti et al., 2008; Schuck et al., 2010; Fig. S9). Since HLE is not influenced by the westerly subtropical jet in the upper troposphere (also clearly seen by the colors of back trajectories in Fig. S9), the summer enhancements of SF_6 observed by the CARIBIC flights are not detected by the flask measurements at HLE. The absence of SF_6 enhancement in summer at HLE confirms weak SF_6 emissions in India. At PBL, the SF_6 seasonal cycle is related to the monsoon circulation and convection (Figs. 9b and S7d). The maximum during November–December (Student's t test, $t = 5.138$, $p < 0.001$; Table S10) is likely due to frequent episodic SF_6-polluted air masses transported from Southeast Asia and China (Fig. S7d).

3.1.5 CO

Carbon monoxide (CO) plays important roles in atmospheric chemistry, as the dominant sink for the hydroxyl radical (OH, the main tropospheric oxidant) and a precursor of tropospheric ozone under high NO_x ($NO+NO_2$) concentrations (Logan et al., 1981; Novelli et al., 1998; Seinfeld and Pandis, 2006). Although CO does not act as a greenhouse gas, it modulates the atmospheric concentrations of CH_4 (the second most abundant anthropogenic greenhouse gas after CO_2) through competition for the OH radicals. At the global scale, it contributes to an indirect positive radiative forcing of 0.23 ± 0.07 W m^{-2} (IPCC, 2013). Additionally, CO is an excellent tracer for combustion processes, with emission sources mainly contributed by incomplete combustion of fossil fuel and biofuels, and by biomass burning (Granier et al., 2011). In India, biofuel and agricultural waste burning account for 70–80 % of the total anthropogenic CO emissions (EDGAR v4.2, 2011; Streets et al., 2003b; Yevich and Logan, 2003).

The time series of CO flask measurements and corresponding smoothed curves are shown in Fig. 10. Over the period

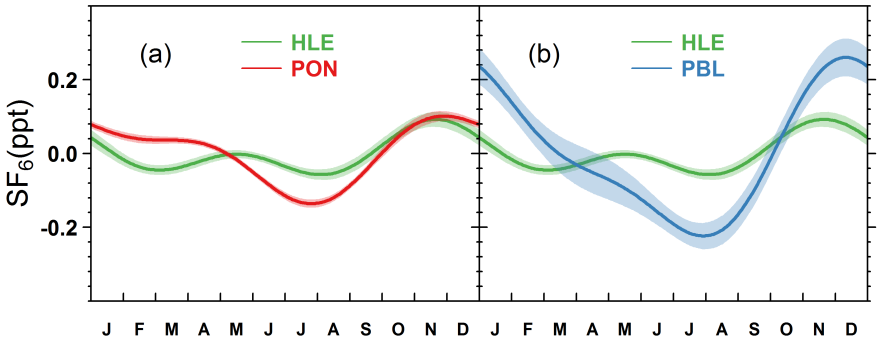

Figure 9. The mean SF_6 seasonal cycles observed at **(a)** HLE and PON and **(b)** HLE and PBL. For each station, the mean seasonal cycle is derived from the harmonics of the smoothed fitting curve in Fig. 8. Shaded area indicates the uncertainty of the mean seasonal cycle calculated from 1 SD of 1000 bootstrap replicates.

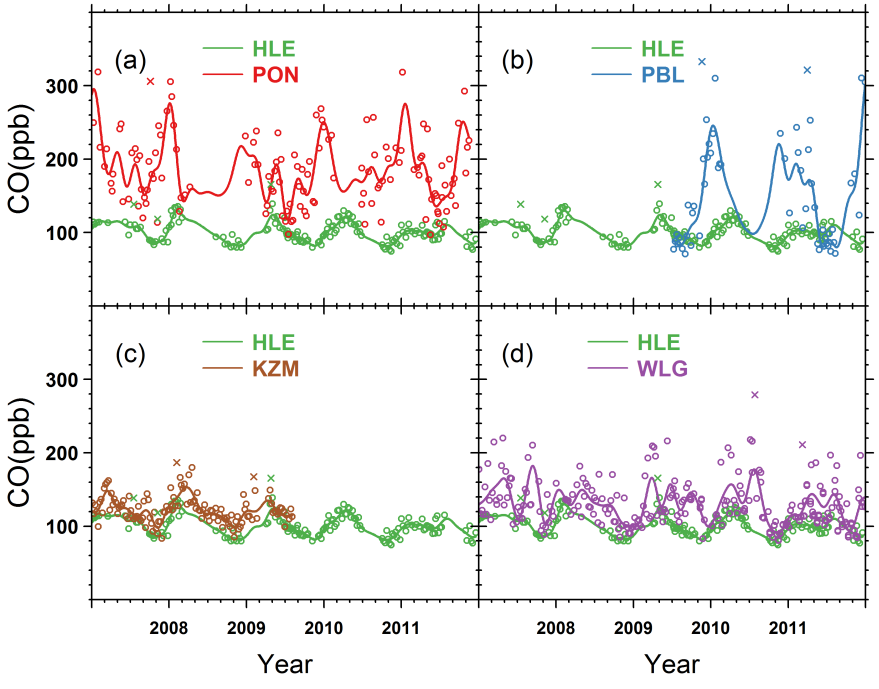

Figure 10. Time series of CO flask measurements at **(a)** HLE and PON, **(b)** HLE and PBL, **(c)** HLE and KZM, and **(d)** HLE and WLG. The open circles denote flask data used to fit the smoothed curves, while the crosses denote discarded flask data lying outside 3 times the residual standard deviations from the smoothed curve fits. For each station, the smoothed curve is fitted using Thoning's method (Thoning et al., 1989) after removing outliers.

of 2007–2011, HLE recorded a slight decrease in CO mole fractions from 104.7 ± 1.4 to 99.4 ± 2.2 ppb, with an annual rate of -2.2 ± 0.0 ppb yr^{-1} ($r^2 = 0.65$, $p = 0.06$). The CO mole fractions at HLE are lower than those at KZM and WLG (Novelli and Masarie, 2014), by on average 18.8 ± 2.5 and 30.2 ± 7.4 ppb, respectively (Table 1, Fig. 10c and d). The positive gradient between KZM, WLG and HLE not only reflects decreasing CO with altitude and the N–S global gradient, but also suggests differences in regional emission sources. For example, compared to HLE, the CO signals at WLG are more influenced by transport of polluted air, especially during summer when about 30 % air masses pass over industrialized and urbanized areas southeast of the station (Zhang et al., 2011). Additionally, the positive CO gradient between KZM, WLG and HLE may be further increased by air masses of northern Siberia origin in summer (Fig. S5), with higher CO emissions from biomass burning and secondary CO from the oxidation of CH_4 and non-CH_4 hydro-

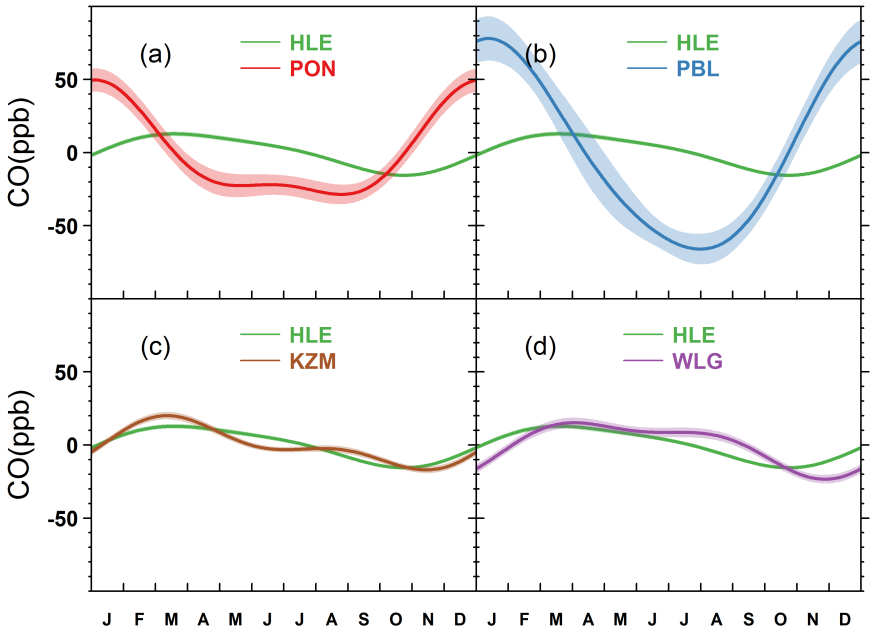

Figure 11. The mean CO seasonal cycles observed at **(a)** HLE and PON, **(b)** HLE and PBL, **(c)** HLE and KZM, and **(d)** HLE and WLG. For each station, the mean seasonal cycle is derived from the harmonics of the smoothed fitting curve in Fig. 10. Shaded area indicates the uncertainty of the mean seasonal cycle calculated from 1 SD of 1000 bootstrap replicates.

carbons (Konovalov et al., 2014). At PON and PBL, the annual mean CO mole fractions are higher than that at HLE by on average 82.4 ± 10.7 and 52.5 ± 8.5 ppb, respectively (Table 1, Fig. 10a and b). The PON and PBL stations are influenced by CO regional emissions, mainly due to biofuel and agricultural burning over South and Southeast Asia (Lelieveld et al., 2001; Streets et al., 2003a, b; Yevich and Logan, 2003). We also note that, for all five stations, the CO time series show larger variability with respect to their corresponding smoothed curves than other species do (see the residual SD (RSD) in Table 1, Fig. 10), as a result of the unevenly distributed CO sources and short atmospheric lifetime (Novelli et al., 1992).

As shown in Fig. 11, the CO seasonal cycle at HLE reaches a maximum in mid-March and a minimum by the end of October, with a peak-to-peak amplitude of 28.4 ± 2.3 ppb (Table 1, Fig. 11). The phase of the mean CO seasonal cycle at HLE generally agrees with the ones observed at KZM and WLG, with a lag of up to 1 month in the timing of seasonal minimum at the two stations (Table 1, Fig. 11c and d). In contrast with the three stations representative of large-scale free tropospheric air masses, the stations at the maritime boundary layer in the mid-to-high Northern Hemisphere observe the lowest CO values in July or August (Novelli et al., 1992, 1998), when the concentration of OH – the major sink of CO – is highest (Logan et al., 1981). The delay in timing of the seasonal CO minimum at the three free troposphere stations in Central and South Asia compared to those boundary layer stations is probably due to the mixing time of regional surface CO emissions and the relatively short lifetime of CO (1–2 months on average). During summer, KZM and WLG sample air masses from Siberia impacted by CO fire emissions (Duncan et al., 2003; Kasischke et al., 2005), and CO-polluted air from urbanized and industrialized areas (Zhang et al., 2011), while HLE is influenced by convective mixing of CO emissions from India, either from anthropogenic sources or oxidation of volatile organic compounds. It is interesting to note that the CO seasonal cycle at HLE does not show an enhancement during JAS as CH_4 and N_2O do (Figs. 5 and 7), possibly as a result of OH oxidation that reduces CO and acts oppositely to vertical transport, and/or differences in seasonal emission patterns between CO and the other two species (Baker et al., 2012). However, the CO enhancement during summer was observed in the upper troposphere over South Asia from the CARIBIC aircraft measurements at flight altitudes 8–12.5 km and Microwave Limb Sounder observations at 100–200 hPa (Li et al., 2005; Jiang et al., 2007a; Schuck et al., 2010). The differences in the CO seasonal cycles at different altitudes suggest faster transport (and younger air masses) at 10 km than at 5 km due to convection, controlling the vertical profile of CO, which makes it difficult to directly compare aircraft measurements in the upper troposphere and column remote sensing observations with surface data.

At PON and PBL, the mean CO seasonal cycles show maxima in the boreal winter and minima in the boreal summer, with peak-to-peak amplitudes of 78.2 ± 11.6 and 144.1 ± 16.0 ppb, respectively (Fig. 11a and b). A strong

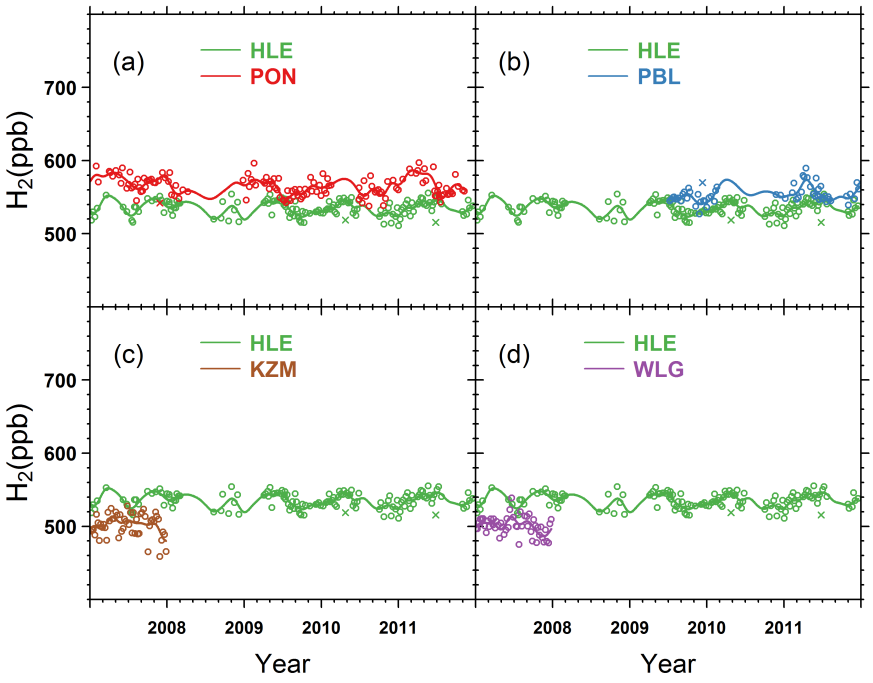

Figure 12. Time series of H_2 flask measurements at **(a)** HLE and PON, **(b)** HLE and PBL, **(c)** HLE and KZM, and **(d)** HLE and WLG. The open circles denote flask data used to fit the smoothed curves, while the crosses denote discarded flask data lying outside 3 times the residual standard deviations from the smoothed curve fits. For each station, the smoothed curve is fitted using Thoning's method (Thoning et al., 1989) after removing outliers.

and positive correlation is found between detrended CO and CH_4 at PON ($r = 0.70$, $p < 0.001$) and PBL ($r = 0.84$, $p < 0.001$), suggesting that the seasonal cycles of both species are dominated by the seasonally varying atmospheric transport. During summer when the southwest monsoon prevails, the surface CO concentrations at PON and PBL are low due to rapid convective uplifting and advection of clean air masses from the ocean. During winter, the two stations are influenced by northeasterly air masses enriched in CO from northeastern India, Southeast Asia and China (back trajectories in Fig. S7e), probably influenced by biofuel and agricultural waste burning in these regions (Yevich and Logan, 2003; Lelieveld et al., 2001).

3.1.6 H_2

Hydrogen (H_2) is the second most abundant reduced trace gas in the troposphere after CH_4, with an average mole fraction of ~ 530 ppb (Novelli et al., 1999). It plays important roles in tropospheric and stratospheric chemistry and indirectly impacts budgets of CH_4, CO and non-methane hydrocarbons (NMHCs) through reaction with OH radicals (Novelli et al., 1999; Ehhalt and Rohrer, 2009). Like CO, H_2 is also a good tracer for incomplete combustion emissions from fossil fuel and biomass/biofuel burning, which are quite extensive in India (Streets et al., 2003b; Yevich and Logan, 2003).

Figure 12 shows the time series of H_2 flask measurements with smoothed curves at HLE, PON, and PBL, respectively. No significant trend was observed at any of the three stations (Table 1, Fig. 12), consistent with the long-term H_2 measurements at other background stations during the last 3 decades (Novelli et al., 1999; Ehhalt and Rohrer, 2009; Grant et al., 2010). For the year 2008, comparing to KZM and WLG (Novelli et al., 2014), HLE recorded higher H_2 mole fractions by ~ 40 ppb, reflecting the latitudinal gradient of H_2 with lower concentrations towards northern high latitudes, due to land uptake by soils (Novelli et al., 1999; Price et al., 2007; Hauglustaine and Ehhalt, 2002; Ehhalt and Rohrer, 2009). Note that these results based on only a 1-year comparison need to be confirmed by extended, more up-to-date data, which are not available yet. At PON and PBL, the annual mean H_2 mole fractions were higher than at HLE by 29.8 ± 4.1 and 21.8 ± 4.6 ppb, respectively (Table 1; Fig. 12). Comparisons with H_2 measurements at Mariana Island, Guam (GMI – 13.39° N, 144.66° E, 0.00 m a.s.l.) (Novelli et al., 2014), another maritime station in the western Pacific at a similar latitude as PON and PBL, also showed positive gradients of ~ 40 ppb (Fig. S13c and d; Table S11), suggesting substantial regional H_2 sources over the footprint area of PBL and PON. During October–March when the NE monsoon prevails, both PON and PBL receive H_2-enriched air masses from South and Southeast Asia, mainly influenced by fossil fuel combustion and biomass burning (Fig. S7f;

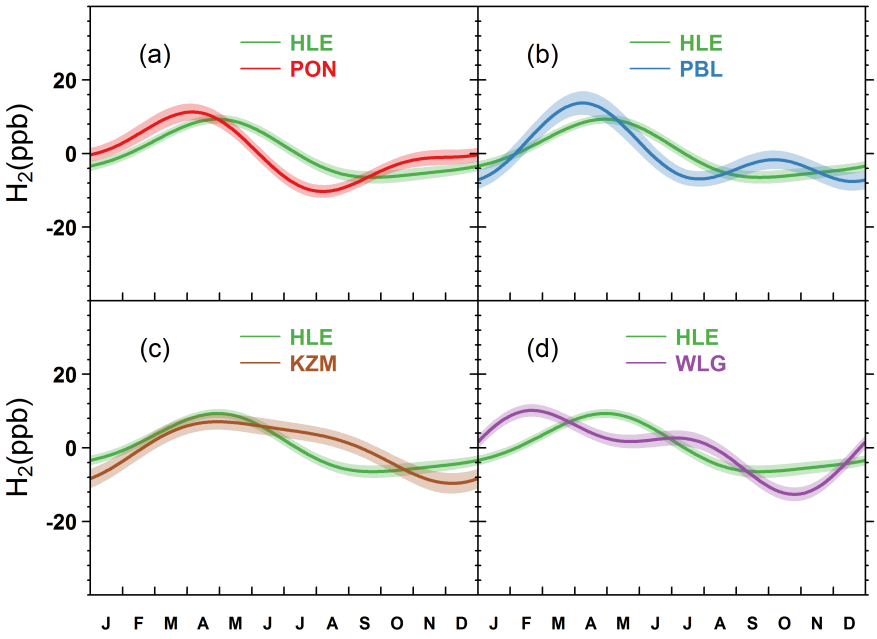

Figure 13. The mean H_2 seasonal cycles observed at **(a)** HLE and PON, **(b)** HLE and PBL, **(c)** HLE and KZM, and **(d)** HLE and WLG. For each station, the mean seasonal cycle is derived from the harmonics of the smoothed fitting curve in Fig. 12. Shaded area indicates the uncertainty of the mean seasonal cycle calculated from 1 SD of 1000 bootstrap replicates.

GFED v3.1; Hauglustaine and Ehhalt, 2002; Price et al., 2007; Ehhalt and Rohrer, 2009; van der Werf et al., 2010). During April–September, with the northward movement of the Intertropical Convergence Zone (ITCZ), the two stations are influenced by advection of air from south of the Equator. For PON, H_2-polluted air masses are occasionally sampled during JAS when the SW monsoon moves over the region of southern India with high population and heavy industry (Fig. S7f; Census India, 2011).

The mean H_2 seasonal cycles for HLE, PON, and PBL are presented in Fig. 13. At HLE, the peak-to-peak H_2 seasonal amplitude is 15.8 ± 2.2 ppb, less than half of the seasonal amplitudes at BMW (39.6 ± 2.6 ppb) and MID (38.0 ± 2.4 ppb) of similar latitudes (Novelli et al., 2014a), and that at WLG (22.8 ± 3.0 ppb) (Figs. 13d and S14a, Tables 1 and S11). The maximum and minimum of H_2 occur in April and September, respectively. The dampening of the H_2 seasonal amplitude with increasing altitude was previously found for another high-altitude continental station at Jungfraujoch, Switzerland (JUN – 46.53° N, 7.98° E, 3580.00 m a.s.l.) (Bond et al., 2011), and was also captured by the GEOS-Chem global chemical transport model (Price et al., 2007). Since the soil sink dominates much of the surface H_2 seasonal cycle in the mid-to-high Northern Hemisphere (Hauglustaine and Ehhalt, 2002; Price et al., 2007; Bousquet et al., 2011; Yver et al., 2011; Yashiro et al., 2011), the smaller amplitude in the H_2 seasonal cycle at HLE may be attributed to the weakened soil sink with increasing altitude due to vertical mixing (Price et al., 2007; Bond et al., 2011).

At PON and PBL, the mean H_2 seasonal cycles are characterized by the peak-to-peak amplitudes of 21.6 ± 3.4 and 21.3 ± 5.0 ppb respectively, comparable to that at GMI (21.5 ± 1.2 ppb) (Tables 1 and S11, Figs. 13a and b and S14b). At PBL, the H_2 maximum in March–April and a secondary increase during September–October coincide with the double biomass burning peaks in each hemisphere – in March for northern tropics, in August/September for southern tropics (van der Werf et al., 2006; Price et al., 2007; Bousquet et al., 2011; Yver et al., 2011). Given that the seasonal variation of soil H_2 uptake is probably small in the tropics (Price et al., 2007; Bousquet et al., 2011; Yver et al., 2011; Yashiro et al., 2011), this bimodal H_2 seasonal cycle at PBL could be related to biomass burning.

3.2 Synoptic variations

In this section we analyze synoptic variations of CO_2, CH_4, and CO by examining correlations between species, after subtracting the smoothed curve from the original data. Ratios of trace gas mole fractions or their enhancements have been widely used in previous studies to partition contributions from different source types and origins (Langenfelds et al., 2002; Paris et al., 2008; Lopez, 2012), to estimate emissions of one species given emissions of another one that is better-known (Gamnitzer et al., 2006; Rivier et al., 2006; Turnbull et al., 2006; Schuck et al., 2010), and to provide valuable constraints on inversion of sources and sinks of trace gases (Xiao et al., 2004; Pison et al., 2009).

3.2.1 $\Delta CH_4/\Delta CO$

Figure 14 shows scatterplots of CH_4 and CO residuals with the orthogonal distance regression lines at HLE, PON, and PBL for different seasons. A significant and positive correlation between CH_4 and CO residuals (hereafter $\Delta CH_4/\Delta CO$, unit ppb ppb^{-1}) is found for all three stations throughout the year. Furthermore, the $\Delta CH_4/\Delta CO$ ratio also shows seasonal variation at each of the three stations. The most prominent feature is the occurrence of maximum slopes in July–September (also October–December at PON), especially at HLE and the generally higher ratios at this station. Wada et al. (2011) and Niwa et al. (2014) also reported increased summer $\Delta CH_4/\Delta CO$ over the western North Pacific, according to the in situ measurements at several surface stations and aircraft flask measurements in the mid-troposphere. The main process for this seasonal variation of $\Delta CH_4/\Delta CO$ might be the enhanced emissions of biogenic CH_4 in summer (e.g., wetland and rice paddy emissions; Streets et al., 2003a; Yan et al., 2003) combined with concurrent lower anthropogenic CO emissions in summer than in winter (due to less residential fuel use for heating, see Streets et al., 2003a). The faster photochemical destruction of CO by increased OH during summer cannot explain such large changes (less than 15 % according to Wada et al., 2011).

At HLE, the $\Delta CH_4/\Delta CO$ ratio varies from 1.2 ± 0.3 to 4.0 ± 1.2 ppb ppb^{-1} throughout the year, with a maximum in JAS, corresponding to the summer monsoon season (Fig. 14a–d). Based on the CARIBIC flights between 10 and 12 km from Frankfurt, Germany to Chennai, India, Baker et al. (2012) derived a $\Delta CH_4/\Delta CO$ ratio in the range 1.88 ± 0.22 to 4.43 ± 0.56 in JAS over South Asia. The maximum $\Delta CH_4/\Delta CO$ observed during summer in the mid-to-upper troposphere may be the result of higher biogenic CH_4 emissions over the Indian subcontinent and lower CO emissions, combined with frequent widespread convective uplift of surface air during the SW monsoon (Schuck et al., 2010; Baker et al., 2012). The CARIBIC flights recorded similar $\Delta CH_4/\Delta CO$ values to HLE, confirming that convection plays a dominant role compared to advection during the SW monsoon season. Outside the SW monsoon season, both the CARIBIC flights and HLE generally did not record strong effects of surface emissions due to the weakened vertical transport. With respect to the $\Delta CH_4/\Delta CO$ ratios for January–March, April–June and October–December, our estimates are 1.5 to 4 times that of the ratios determined for air masses with signatures of fossil fuel combustion, according to several aircraft and ground observations in East and Southeast Asia (Table S12; Sawa et al., 2004; Lai et al., 2010; Wada et al., 2011; Niwa et al., 2014), which rules out fossil fuel combustion as an explanation for the higher ratios. Our ratios are comparable to the $\Delta CH_4/\Delta CO$ values inferred for air masses of Siberian origin during winter (Table S12; Harris et al., 2000; Chi et al., 2013), and we also obtain similar estimates of $\Delta CH_4/\Delta CO$ from the flask measurements at KZM over the study period ($\Delta CH_4/\Delta CO$ ratios for KZM are 0.8 ± 0.2, 1.7 ± 0.2 and 1.5 ± 0.3 ppb ppb^{-1} for AMJ, OND and JFM, respectively), which are influenced by air masses originating from northern Africa, the Middle East, and Central Asia as seen at HLE (see back trajectories in Fig. S5). Given that oil and gas production accounts for 50–70 % of CH_4 emissions in these regions (EDGAR v4.2, 2011), and that over dry areas the daytime boundary layer is higher favoring injection of surface emissions into the troposphere, the preferential enrichment in CH_4 relative to CO at HLE may tentatively be attributed to fossil CH_4 emissions over gas extraction regions and transported eastwards by westerlies (Harris et al., 2000; Tohjima et al., 1996).

At PON and PBL, the $\Delta CH_4/\Delta CO$ ratios are in general considerably higher than 0.3 for all seasons, putting them in the range of ratios indicative of urban/industrial sources (Table S12; Harriss et al., 1994; Sawa et al., 2004; Xiao et al., 2004; Bakwin et al., 1995; Lai et al., 2010; Wada et al., 2011; Niwa et al., 2014). However, this does not rule out contributions from biomass/biofuel burning with emissions having a typical $\Delta CH_4/\Delta CO$ ratio less than 0.3 (Mauzerall et al., 1998; Andreae and Merlet, 2001; Mühle et al., 2002). Considering that biofuel and agriculture waste burning are the primary energy sources in rural India (Streets et al., 2003a; Yevich and Logan, 2003; Venkataraman et al., 2005), CO emissions from biofuel burning must be substantial (Lelieveld et al., 2001). This is the case for NE India located upwind of PON and PBL when the NE monsoon prevails during December–March. Nevertheless, the relatively low $\Delta CH_4/\Delta CO$ derived from biomass/biofuel burning could be increased by CH_4 emissions from livestock with similarly distributed sources (EDGAR v4.2, 2011). Emissions of both trace gases from livestock and biomass/biofuel burning in the Indian subcontinent compiled by EDGAR v4.2 (2011) also indicate a CH_4-to-CO ratio of 0.64–0.69 over the period of 2000–2008, close to the atmospheric measurements of $\Delta CH_4/\Delta CO$ at PON and PBL during JFM (Fig. 14h and l).

3.2.2 $\Delta CH_4/\Delta CO_2$

The $\Delta CH_4/\Delta CO_2$ ratios are strongly influenced by the high variability of CO_2 and the interpretation is complex. Unlike the positive correlation between CH_4 and CO consistently observed at all three stations, the relationships between CH_4 and CO_2 residuals exhibit scattering and differences in the residual slopes for different stations and seasons (Fig. 15). At HLE, no significant correlations are found during AMJ, JAS, and OND (Fig. 15a–c) because CH_4 and CO_2 have distinct biogenic and/or photochemical sources and sinks over the northern mid-latitudes. During JFM when biogenic CO_2 fluxes and anthropogenic emissions to the atmosphere are positive, there is a significant and positive relationship between CH_4 and CO_2, with a $\Delta CH_4/\Delta CO_2$ ratio of 45.6 ± 1846.8 ppb ppm^{-1} ($r =$

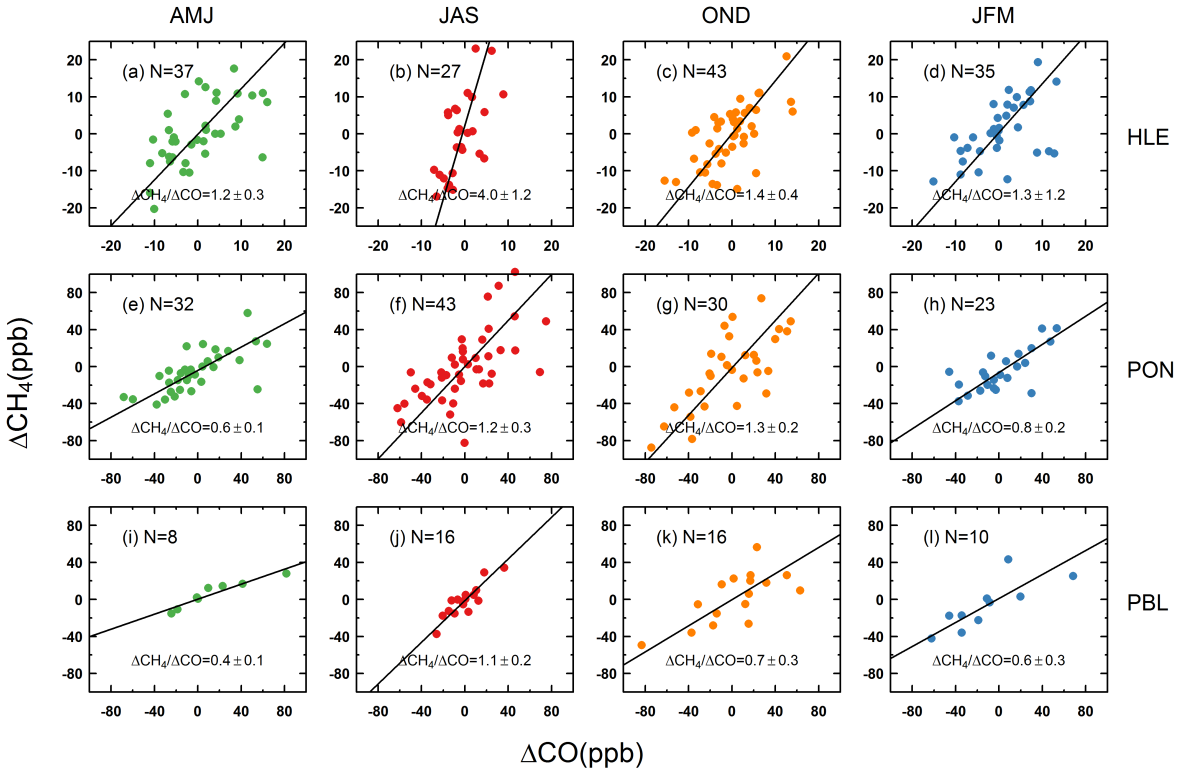

Figure 14. The relationships between ΔCH_4 and ΔCO at HLE **(a–d)**, PON **(e–h)**, and PBL **(i–l)** for April–June (AMJ), July–September (JAS), October–December (OND), and January–March (JFM). For each panel, ΔCH_4 and ΔCO are estimated as residuals from smoothed curves. The $\Delta CH_4/\Delta CO$ ratio is the slope of the fitting line from the orthogonal distance regression, with the SD calculated from 1000 bootstrap replications.

0.37, $p = 0.03$; Fig. 15d). This value is close to the ratio of CH_4 and CO_2 anthropogenic emissions over northern Africa (39.1–46.2 mmol mol^{-1}), Central Asia (44.4–49.5 mmol mol^{-1}) and to a lesser degree the Middle East (25.8–28.4 mmol mol^{-1}) during the period of 2000–2010 (EDGAR v4.2, 2011), corresponding to the back trajectories reaching HLE (Fig. 1a). It should be noted that this estimate of $\Delta CH_4/\Delta CO_2$ is subject to large uncertainty according to the standard deviation calculated with 1000 bootstrap replications (Fig. 15d), implying that CH_4 and CO_2 sources of various types and origins influence the HLE records.

At PON, in contrast to HLE, positive correlations occur between CH_4 and CO_2 residuals for all seasons except OND, with a $\Delta CH_4/\Delta CO_2$ ratio of 6.7 ± 2.4 ppb ppm^{-1} ($r = 0.72$, $p < 0.001$) in AMJ and 8.5 ± 0.9 ppb ppm^{-1} in JAS ($r = 0.74$, $p < 0.001$), respectively (Fig. 15e and f). The relatively narrow ranges of slopes compared to those for HLE and PBL likely suggest co-located urban and industrial sources in southern India upwind of PON during April–September (see back trajectories in Fig. 1a). Emissions from biofuel burning could be a common source for both CH_4 and CO_2, given the substantial biofuel use in southern India (Yevich and Logan, 2003) and the biofuel burning emission ratio of CH_4 and CO_2 derived from previous studies (5–10 mmol mol^{-1}; Andreae and Merlet, 2001). Note that the CARIBIC flask measurements over India south of 20° N indicate a negative correlation between CH_4 and CO_2 at the altitudes of 10–12 km during July–September 2008 ($r = -0.80$, $p = 0.002$; Fig. S15a), interpreted as the concurrent strong uptake of CO_2 with enhanced emissions of CH_4 during the SW monsoon. During JFM when the NE monsoon predominates, CH_4 is positively correlated with CO_2 with a $\Delta CH_4/\Delta CO_2$ ratio of 31.9 ± 1635.7 ppb ppm^{-1} ($r = 0.45$, $p = 0.02$; Fig. 15h). Like at HLE, this ratio is subject to large uncertainty due to variability in CH_4 and CO_2 sources. The ratio based on the CARIBIC observations in the upper troposphere (10–12 km) is 23.5 ± 41.4 ppb ppm^{-1} ($r = 0.67$, $p = 0.004$; Fig. S15b). The inconsistency of the $\Delta CH_4/\Delta CO_2$ ratios estimated from the two data sets suggest that the flask measurements at the surface station PON provide more specific information for constraining estimates of regional CH_4 and CO_2 fluxes.

Finally, at PBL, the prominent feature of the CH_4–CO_2 relationship is the significant and negative correlation observed during JAS, with a $\Delta CH_4/\Delta CO_2$ ratio of -14.6 ± 16.4 ppb ppm^{-1} ($r = -0.73$, $p = 0.007$; Fig. 15j). Since the time series of flask measurements at PBL is relatively short and has large data gaps (Fig. S3), correlations between trace gases could be influenced by abnormal pollution

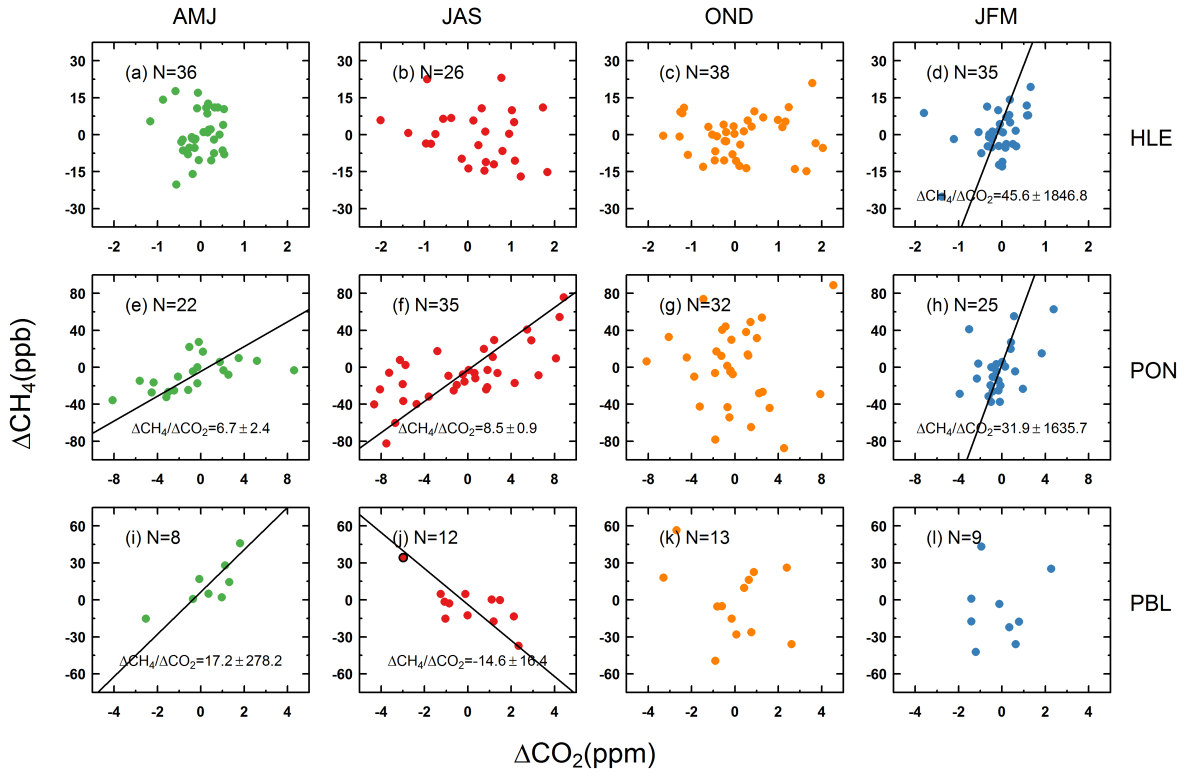

Figure 15. The relationships between ΔCH_4 and ΔCO_2 at HLE **(a–d)**, PON **(e–h)**, and PBL **(i–l)** for April–June (AMJ), July–September (JAS), October–December (OND), and January–March (JFM). For each panel, ΔCH_4 and ΔCO_2 are estimated as residuals from smoothed curves. The $\Delta CH_4/\Delta CO_2$ ratio is the slope of the fitting line from the orthogonal distance regression, with the SD calculated from 1000 bootstrap replications. For ΔCH_4 and ΔCO_2 values that are not significantly correlated, the fitting line is not plotted.

events. For example, excluding the event with CH_4 residuals $> +20$ ppb (corresponding to the observation at PBL on 16 September 2009, the point marked with black-outlined circle in Fig. 15j) would substantially decrease the strength of the negative correlation between CH_4 and CO_2 ($r = -0.54$, $p = 0.09$). We will investigate the CH_4-enriched event further in Sect. 3.3.

3.2.3 $\Delta CO/\Delta CO_2$

As shown in Fig. 16, at HLE, CO is positively correlated with CO_2 during AMJ, with a $\Delta CO/\Delta CO_2$ ratio of 35.8 ± 12.1 ppb ppm^{-1} ($r = 0.53$, $p = 0.001$; Fig. 16a). During JFM, there is no significant relationship between CO and CO_2 ($r = 0.15$, $p = 0.39$; Fig. 16d). However, when excluding an abnormal event with $\Delta CO_2 = -1.8$ ppm on 8 January 2007 (the point marked with black-outlined circle in Fig. 16d), there is a significant and positive correlation between CO and CO_2, with a $\Delta CO/\Delta CO_2$ ratio of 55.7 ± 259.1 ppb ppm^{-1} ($r = 0.40$, $p = 0.02$; the red solid line in Fig. 16d). This ratio is less than half the emission ratio of CO to CO_2 from forest/grassland biomass burning (Mauzerall et al., 1998; Andreae and Merlet, 2001), but higher than ratios of anthropogenic combustion sources in developed countries that are typically in the range of 10–15 ppb ppm^{-1} (e.g., Suntharalingam et al., 2004; Wada et al., 2011; Takegawa et al., 2004). This could be attributed not only to the lower combustion efficiency of fuels in northern Africa, the Middle East, and Central Asia where air masses at HLE originate from, but also to additional contributions from biofuel burning with relatively high CO to CO_2 emission ratios (e.g., fuelwood, charcoal, agricultural residuals; Andreae and Merlet, 2001). Additionally, the relatively high $\Delta CO/\Delta CO_2$ in JFM compared to AMJ may further indicate a contribution of CO emissions from residential biofuel burning in winter (Wada et al., 2011), especially in developing countries within the footprint area.

At PON, a positive and significant correlation between CO and CO_2 is found during AMJ, with a $\Delta CO/\Delta CO_2$ ratio of 13.4 ± 76.8 ppb ppm^{-1} ($r = 0.46$, $p = 0.03$; Fig. 16e). This ratio is similar to the ratios determined for air masses influenced by both fossil fuel emissions and biomass/biofuel burning during the same seasons. For example, based on the in situ measurements in the upper troposphere during the CARIBIC flights between southern China and Philippines in April 2007, Lai et al. (2010) reported $\Delta CO/\Delta CO_2$ ratios of 15.6–29.3 ppb ppm^{-1} during pollution events influenced by both biomass/biofuel burning and fossil fuel combustion in

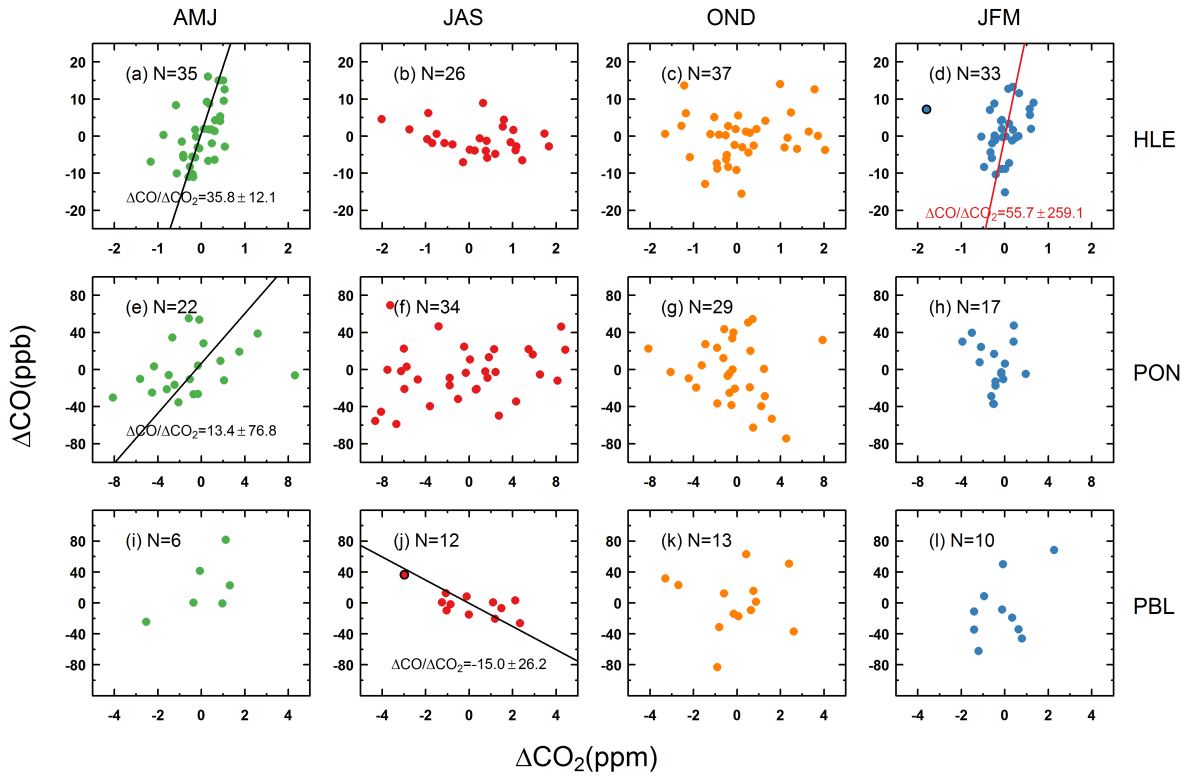

Figure 16. The relationships between ΔCO and ΔCO_2 at HLE **(a–d)**, PON **(e–h)**, and PBL **(i–l)** for April–June (AMJ), July–September (JAS), October–December (OND), and January–March (JFM). For each panel, ΔCO and ΔCO_2 are estimated as residuals from smoothed curves. The $\Delta CO / \Delta CO_2$ ratio is the slope of the fitting line from the orthogonal distance regression, with the SD calculated from 1000 bootstrap replications. For ΔCO and ΔCO_2 values that are not significantly correlated, the fitting line is usually not plotted.

Indochina. At PBL, CO is significantly and negatively correlated with CO_2 during JAS ($r = -0.68$, $p = 0.01$; Fig. 16j). However, we note that the abnormal CH_4 event discussed in Sect. 3.2.2 is enriched in CO as well, and the negative relationship between CO and CO_2 would no longer exist if we removed the event ($r = -0.45$, $p = 0.16$). The simultaneous enhancement of CO and CH_4 may suggest possible influences of biomass burning episodes, which we will explore in detail in Sect. 3.3. During JFM, no significant relationship is found between CO and CO_2 for PON or PBL (Fig. 16h and l).

3.3 Elevated CH_4 and CO events at PBL

In this section, we discuss two elevated CH_4 and CO events at PBL during the SW monsoon season. Significant enhancements of CH_4 and CO were observed on 16 September 2009 (29 July 2011), with residuals from smoothed curves as high as 34.2 (29.2) ppb and 36.2 (17.9) ppb for CH_4 and CO, respectively. We further analyzed CH_4 and CO measurements at Bukit Kototabang (BKT – 0.20° S, 100.32° E, 845.00 m a.s.l.), Indonesia, located upwind of PBL when the southwest monsoon prevails. The flask measurements at BKT detected enhanced CH_4 and CO with a magnitude of 38.0 and 66.1 ppb on 8 September 2009, about 1 week before the occurrence of the first CH_4 and CO event at PBL (Fig. 17a). The in situ measurements at BKT also showed CH_4 and CO enhancements about 1 week before the second event at PBL, lasting over the period of 17 July–21 July 2011 (Fig. 17b). The co-occurrence of the two abnormal CH_4 and CO events at PBL and BKT suggests possible influences of polluted air masses with common sources and origins. Moreover, the fire radiative power (FRP, $mW\,m^{-2}$) during the sampling dates implies that the two abnormal CH_4 and CO events could be related to fire emissions in Indonesia (GFAS product version 1.0; Kaiser et al., 2012; Fig. S16). Note that the mechanisms we propose for the abnormal CH_4 and CO events and the possible linkage between PBL and BKT during the SW monsoon season are still speculative. Model experiments are needed to further confirm these hypotheses.

4 Conclusions

In this paper we present the results of flask measurements of CO_2, CH_4, N_2O, SF_6, CO, and H_2 at three stations in India: Hanle (HLE), Pondicherry (PON) and Port Blair (PBL), over the period of 2007–2011. Of these three stations, HLE is located at high altitude and is regarded as a continental

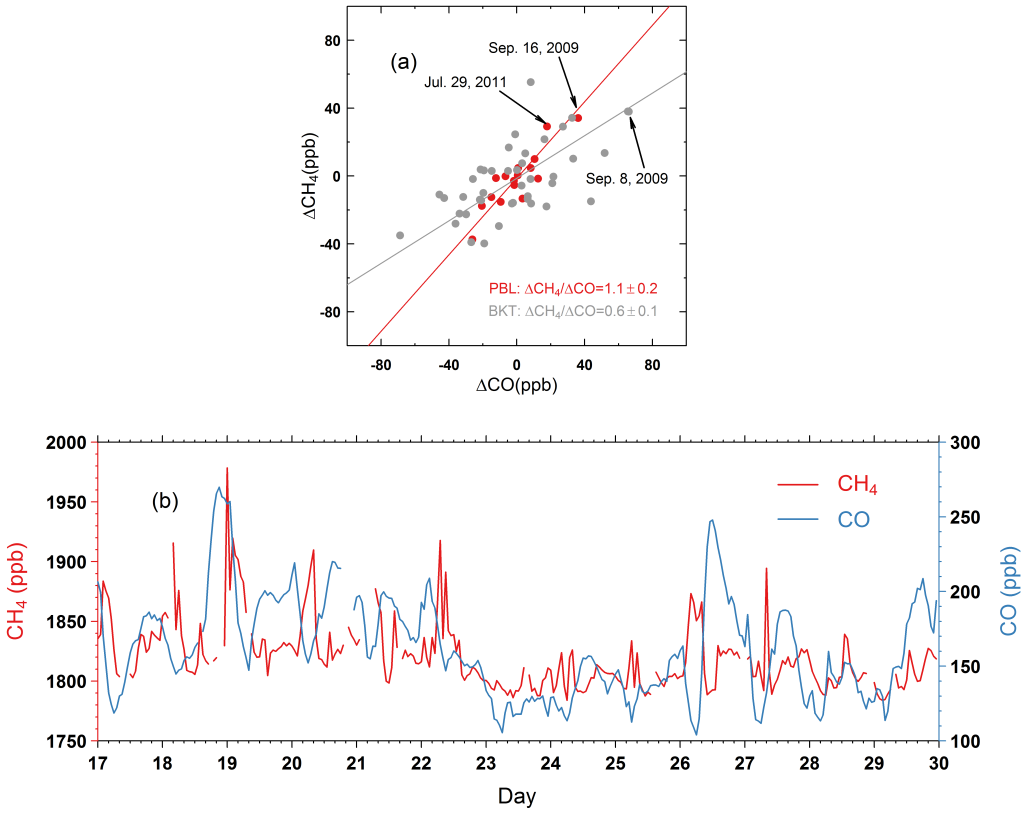

Figure 17. (a) The relationship between ΔCH_4 and ΔCO at PBL (colored by red) and BKT (colored by grey) during July–September (JAS) over the period of 2007–2011. ΔCH_4 and ΔCO are estimated as residuals from smoothed curves. The $\Delta CH_4/\Delta CO$ ratio is the slope of the fitting line from orthogonal distance regression (ODR), with the SD calculated from 1000 bootstrap replications. Two abnormal events at PBL are labeled, with enhancements of CH_4 and CO on 16 September 2009 and 29 July 2011, respectively. Enhancements of CH_4 and CO are also observed at BKT on 8 September 2009. **(b)** Hourly CH_4 and CO measurements at BKT in July 2011. Enhancements of CH_4 and CO are observed during 17–21 July 2011.

background station in the mid-latitude of the Northern Hemisphere; PON is a tropical surface station located on the southeast coast of India, while PBL is an oceanic station located on the Andaman Islands, of similar latitude to PON. With a total of 188, 185, and 63 flask pair samples collected respectively from HLE, PON and PBL between 2007 and 2011 (for PBL between 2009 and 2011), and analyzed at LSCE, the program is an important logistical and analytical effort to produce a unique data set of atmospheric trace gas observations over the Indian subcontinent. The observed records will serve as an important source of information to infer regional patterns of trace gas fluxes and atmospheric transport in this under-documented region. Several conclusions and implications are drawn from the first analyses of the data sets.

The annual gradients of the atmospheric mole fractions observed at PON and PBL, with respect to HLE as a reference, suggest significant emission sources of CO_2, CH_4, N_2O, CO, and H_2 over the footprints of those stations. In particular, the annual mean N_2O mole fractions at PON and PBL are higher than at HLE by 3.1 ± 0.3 and 3.8 ± 1.7 ppb, notably larger than the typical N_2O gradients observed between stations in Europe or North America, indicating substantial N_2O emissions. The analyses of the atmospheric mole fractions with back trajectories at the three stations further confirmed emission sources from southern and northeastern India, and SE Asia, all of which are highly populous and have high demand for food and energy, and thus high emissions from industrial, residential, and/or agricultural sectors. On the other hand, despite substantial anthropogenic GHG emissions in India (whether based on national inventories or atmospheric observations), unlike the USA and countries of the EU, its SF_6 emissions are rather weak.

The seasonal cycles for each trace gas reflect not only the seasonal variations of natural sources/sinks and anthropogenic emissions over the Indian subcontinent, but also the seasonally varying atmospheric transport, especially the monsoon circulations (including convection). Strong influences of the monsoon circulations are well depicted by the contrasting phases of CH_4 seasonal cycles between HLE and PON/PBL. At HLE, the distinct CH_4 maximum during June–September is likely related to the enhanced biogenic CH_4 emissions from wetlands and rice paddies in summer, com-

bined with deep convection associated with the SW monsoon that mixes surface emissions into the mid-to-upper troposphere. By contrast, the CH_4 seasonal cycles at PON and PBL have seasonal minima during the SW monsoon season, reflecting influences of southern hemispheric air depleted in CH_4 transported at low altitudes, as well as high rates of OH oxidation. Covariance between species variations at the synoptic scale further helps identification and attribution of different sources and sinks, like fossil fuel combustion, biofuel burning and biogenic emissions. Additionally, measurements of $\delta^{13}C$–CO_2 have recently begun for HLE, and the 4-D distributions of CO_2 and CH_4 have been realistically simulated using a chemical transport model (LMDZ-OR-INCA, Hauglustaine et al., 2004; Folberth et al., 2006) zoomed over South and East Asia (manuscript in preparation). Both of them may serve as valuable tools for disentangling and quantifying contributions of different sources and meteorology to trace gas signals.

Apart from the flask measurements of trace gases presented in this study for the three stations, in situ continuous measurements of CO_2 and CH_4 have also been undertaken at HLE, PON and PBL in parallel, which will considerably contribute to the value of the stations through high-frequency air sampling. While the three stations have the potential to provide useful constraints on estimates of trace gas fluxes over southern and northeastern India (for example, Swathi et al. (2013) reported considerable reduction in the uncertainty of inverted CO_2 fluxes over temperate Eurasia by the inclusion of measurements at HLE), the monitoring network requires further expansion to sample air masses from other parts of the Indian subcontinent. Recently a few other atmospheric ground stations have been established in western India (Bhattacharya et al., 2009; Tiwari et al., 2011, 2014; Tiwari and Kumar, 2012) and the Himalayas (Kumar et al., 2010; Ganesan et al., 2013), with their concentration footprints covering central India (e.g., the Sinhagad station; Tiwari et al., 2014; Tiwari and Kumar, 2012), the Indo-Gangetic Plain and a large extent of the Himalayas (e.g., the Darjeeling station; Ganesan et al., 2013). More efforts are needed to develop a comprehensive observation network with adequate spatial and temporal coverage in this region.

The Supplement related to this article is available online at doi:10.5194/acp-15-9819-2015-supplement.

Acknowledgements. This study was initiated within the framework of CaFICA-CEFIPRA project (2809-1). X. Lin acknowledges PhD funding support from AIRBUS D&S and ESF TTorch Short Visiting Grant for the 1st ICOS Science Conference (no. 6849). P. Ciais acknowledges support of the Synergy grant ERC-2013-SyG-610028 IMBALANCE-P of the European Research Council. The authors thank the helpful engineers and staff of the Indian Astronomical Observatory, Hanle, and Manil Kumar, Shambhulinga and Prabhath Prabhu, who helped in flask sampling at Pondicherry University, B. Parmeshwar from the National Institute of Ocean Technology for operating and maintaining the facilities in the stations. We also acknowledge the LSCE staff (L. Klenov, A. Crevier, B. Gal, C. Peureux, M. Grand, L. Hogrel, V. Bazantay and A. Orgun) in charge of RAMCES network logistics, measurements, and data processing.

Edited by: E. Harris

References

Andreae, M. O. and Merlet, P.: Emission of trace gases and aerosols from biomass burning, Global Biogeochem. Cy., 15, 955–966, doi:10.1029/2000gb001382, 2001.

Attri, S. D. and Tyagi, A.: Climate Profile of India: Contribution to the Indian Network of Climate Change Assessment (NATIONAL COMMUNICATION-II) Minitry of Environment and Forests, Met Monograph No. Environment Meteorology-01/2010, India Meteorological Department, Ministry of Earth Sciences, New Delhi, 2010.

Babu, S. S., Chaubey, J. P., Krishna Moorthy, K., Gogoi, M. M., Kompalli, S. K., Sreekanth, V., Bagare, S. P., Bhatt, B. C., Gaur, V. K., Prabhu, T. P., and Singh, N. S.: High altitude (4520 m amsl) measurements of black carbon aerosols over western trans-Himalayas: Seasonal heterogeneity and source apportionment, J. Geophys. Res.-Atmos., 116, D24201, doi:10.1029/2011jd016722, 2011.

Baker, A. K., Schuck, T. J., Brenninkmeijer, C. A. M., Rauthe-Schöch, A., Slemr, F., van Velthoven, P. F. J., and Lelieveld, J.: Estimating the contribution of monsoon-related biogenic production to methane emissions from South Asia using CARIBIC observations, Geophys. Res. Lett., 39, L10813, doi:10.1029/2012gl051756, 2012.

Bakwin, P. S., Tans, P. P., Zhao, C., Ussler, W., and Quesnell, E.: Measurements of carbon dioxide on a very tall tower, Tellus B, 47, 535–549, doi:10.1034/j.1600-0889.47.issue5.2.x, 1995.

Bakwin, P. S., Tans, P. P., Hurst, D. F., and Zhao, C.: Measurements of carbon dioxide on very tall towers: results of the NOAA/CMDL program, Tellus B, 50B, 401–415, 1998.

Bange, H. W., Andreae, M. O., Lal, S., Law, C. S., Naqvi, S. W. A., Patra, P. K., Rixen, T., and Upstill-Goddard, R. C.: Nitrous oxide emissions from the Arabian Sea: A synthesis, Atmos. Chem. Phys., 1, 61–71, doi:10.5194/acp-1-61-2001, 2001.

Bhattacharya, S. K., Borole, D. V., Francey, R. J., Allison, C. E., Steele, L. P., Krummel, P. B., Langenfelds, R., Masarie, K. A., Tiwari, Y. K., and Patra, P. K.: Trace gases and CO_2 isotope records from Cabo de Rama, India, Curr. Sci., 97, 1336–1344, 2009.

Bond, S. W., Vollmer, M. K., Steinbacher, M., Henne, S., and Reimann, S.: Atmospheric molecular hydrogen (H_2): observations at the high-altitude site Jungfraujoch, Switzerland, Tellus B, 63, 64–76, doi:10.1111/j.1600-0889.2010.00509.x, 2011.

Bousquet, P., Yver, C., Pison, I., Li, Y. S., Fortems, A., Hauglustaine, D., Szopa, S., Rayner, P. J., Novelli, P., Langenfelds, R., Steele, P., Ramonet, M., Schmidt, M., Foster, P., Morfopoulos, C., and Ciais, P.: A three-dimensional synthesis inversion of the molecular hydrogen cycle: Sources and sinks budget and implications for the soil uptake, J. Geophys. Res.-Atmos., 116, D01302, doi:10.1029/2010jd014599, 2011.

Busenberg, E. and Plummer, L. N.: Dating young groundwater with sulfur hexafluoride: Natural and anthropogenic sources of sulfur hexafluoride, Water Resour. Res., 36, 3011–3030, doi:10.1029/2000WR900151, 2000.

Census India, Ministry of Home Affairs, Government of India: 2011 Census Data – Population Enumeration Data (Final Population), available at: http://www.censusindia.gov.in/2011census/population_enumeration.html (last access: 9 August 2014), 2011.

Chi, X., Winderlich, J., Mayer, J.-C., Panov, A. V., Heimann, M., Birmili, W., Heintzenberg, J., Cheng, Y., and Andreae, M. O.: Long-term measurements of aerosol and carbon monoxide at the ZOTTO tall tower to characterize polluted and pristine air in the Siberian taiga, Atmos. Chem. Phys., 13, 12271–12298, doi:10.5194/acp-13-12271-2013, 2013.

Dlugokencky, E. J., Myers, R. C., Lang, P. M., Masarie, K. A., Crotwell, A. M., Thoning, K. W., Hall, B. D., Elkins, J. W., and Steele, L. P.: Conversion of NOAA atmospheric dry air CH_4 mole fractions to a gravimetrically prepared standard scale, J. Geophys. Res.-Atmos., 110, D18306, doi:10.1029/2005jd006035, 2005.

Dlugokencky, E. J., Lang, P. M., Crotwell, A. M., Masarie, K. A., and Crotwell, M. J.: Atmospheric Methane Dry Air Mole Fractions from the NOAA ESRL Carbon Cycle Cooperative Global Air Sampling Network, 1983–2013, Version: 2014-06-24, available at: ftp://aftp.cmdl.noaa.gov/data/trace_gases/ch4/flask/surface/ (last access: 11 December 2014), 2014a.

Dlugokencky, E. J., Lang, P. M., Masarie, K. A., Crotwell, A. M., and Crotwell, M. J.: Atmospheric Carbon Dioxide Dry Air Mole Fractions from the NOAA ESRL Carbon Cycle Cooperative Global Air Sampling Network, 1968–2013, Version: 2014-06-27, available at: ftp://aftp.cmdl.noaa.gov/data/trace_gases/co2/flask/surface/ (last access: 11 December 2014), 2014b.

Draxler, R. R. and Rolph, G. D.: HYSPLIT (HYbrid Single-Particle Lagrangian Integrated Trajectory), Model access via NOAA ARL READY website, http://www.arl.noaa.gov/ready/hysplit4.html (last access: 9 January 2014), NOAA Air Resources Laboratory, Silver Spring, MD, 2003.

Duncan, B. N., Martin, R. V., Staudt, A. C., Yevich, R., and Logan, J. A.: Interannual and seasonal variability of biomass burning emissions constrained by satellite observations, J. Geophys. Res.-Atmos., 108, 4100, doi:10.1029/2002jd002378, 2003.

EDGAR v4.2: EC-JRC/PBL (European Commission, Joint Research Centre/Netherlands Environmental Assessment Agency): Emission Database for Global Atmospheric Research (EDGAR), release version 4.2: available at: http://edgar.jrc.ec.europa.eu (last access: 16 August 2014), 2011.

Ehhalt, D. H. and Rohrer, F.: The tropospheric cycle of H_2: a critical review, Tellus B, 61, 500–535, doi:10.1111/j.1600-0889.2009.00416.x, 2009.

Fang, S.-X., Zhou, L.-X., Masarie, K. A., Xu, L., and Rella, C. W.: Study of atmospheric CH_4 mole fractions at three WMO/GAW stations in China, J. Geophys. Res.-Atmos., 118, 4874–4886, doi:10.1002/jgrd.50284, 2013.

Fang, S. X., Zhou, L. X., Tans, P. P., Ciais, P., Steinbacher, M., Xu, L., and Luan, T.: In situ measurement of atmospheric CO_2 at the four WMO/GAW stations in China, Atmos. Chem. Phys., 14, 2541–2554, doi:10.5194/acp-14-2541-2014, 2014.

Folberth, G. A., Hauglustaine, D. A., Lathière, J., and Brocheton, F.: Interactive chemistry in the Laboratoire de Météorologie Dynamique general circulation model: model description and impact analysis of biogenic hydrocarbons on tropospheric chemistry, Atmos. Chem. Phys., 6, 2273–2319, doi:10.5194/acp-6-2273-2006, 2006.

Gadgil, S.: The Indian Monsoon and its variability, Annu. Rev. Earth Planet Sci., 31, 429–467, doi:10.1146/annurev.earth.31.100901.141251, 2003.

Gamnitzer, U., Karstens, U., Kromer, B., Neubert, R. E. M., Meijer, H. A. J., Schroeder, H., and Levin, I.: Carbon monoxide: A quantitative tracer for fossil fuel CO_2?, J. Geophys. Res.-Atmos., 111, D22302, doi:10.1029/2005jd006966, 2006.

Ganesan, A. L., Chatterjee, A., Prinn, R. G., Harth, C. M., Salameh, P. K., Manning, A. J., Hall, B. D., Mühle, J., Meredith, L. K., Weiss, R. F., O'Doherty, S., and Young, D.: The variability of methane, nitrous oxide and sulfur hexafluoride in Northeast India, Atmos. Chem. Phys., 13, 10633–10644, doi:10.5194/acp-13-10633-2013, 2013.

Garg, A., Shukla, P. R., and Upadhyay, J.: N_2O emissions of India: an assessment of temporal, regional and sector trends, Clim. Change, 110, 755–782, doi:10.1007/s10584-011-0094-9, 2012.

Goswami, B. N.: South Asian Monsoon, in: Intraseasonal variability in the Atmosphere-Ocean Climate System, edited by: Lau, W. K. M. and Waliser, D. E., Springer & Praxis Publishing, Chichester, UK, 2005.

Granier, C., Bessagnet, B., Bond, T., D'Angiola, A., Denier van der Gon, H., Frost, G., Heil, A., Kaiser, J., Kinne, S., Klimont, Z., Kloster, S., Lamarque, J.-F., Liousse, C., Masui, T., Meleux, F., Mieville, A., Ohara, T., Raut, J.-C., Riahi, K., Schultz, M., Smith, S., Thompson, A., van Aardenne, J., van der Werf, G., and van Vuuren, D.: Evolution of anthropogenic and biomass burning emissions of air pollutants at global and regional scales during the 1980–2010 period, Clim. Change, 109, 163–190, doi:10.1007/s10584-011-0154-1, 2011.

Grant, A., Witham, C. S., Simmonds, P. G., Manning, A. J., and O'Doherty, S.: A 15 year record of high-frequency, in situ measurements of hydrogen at Mace Head, Ireland, Atmos. Chem. Phys., 10, 1203–1214, doi:10.5194/acp-10-1203-2010, 2010.

Hall, B. D., Dutton, G. S., and Elkins, J. W.: The NOAA nitrous oxide standard scale for atmospheric observations, J. Geophys. Res.-Atmos., 112, D09305, doi:10.1029/2006jd007954, 2007.

Harris, J. M., Dlugokencky, E. J., Oltmans, S. J., Tans, P. P., Conway, T. J., Novelli, P. C., Thoning, K. W., and Kahl, J. D. W.: An interpretation of trace gas correlations during Barrow, Alaska, winter dark periods, 1986–1997, J. Geophys. Res.-Atmos., 105, 17267–17278, doi:10.1029/2000jd900167, 2000.

Harriss, R. C., Sachse, G. W., Collins, J. E., Wade, L., Bartlett, K. B., Talbot, R. W., Browell, E. V., Barrie, L. A., Hill, G. F., and Burney, L. G.: Carbon monoxide and methane over Canada: July–August 1990, J. Geophys. Res.-Atmos., 99, 1659–1669, doi:10.1029/93jd01906, 1994.

Haszpra, L., Barcza, Z., Hidy, D., Szilágyi, I., Dlugokencky, E., and Tans, P.: Trends and temporal variations of major greenhouse gases at a rural site in Central Europe, Atmos. Environ., 42, 8707–8716, doi:10.1016/j.atmosenv.2008.09.012, 2008.

Hauglustaine, D. A. and Ehhalt, D. H.: A three-dimensional model of molecular hydrogen in the troposphere, J. Geophys. Res.-Atmos., 107, 4330, doi:10.1029/2001jd001156, 2002.

Hauglustaine, D. A., Hourdin, F., Jourdain, L., Filiberti, M. A., Walters, S., Lamarque, J. F., and Holland, E. A.: Interactive chemistry in the Laboratoire de Météorologie Dynamique general circulation model: Description and background tropospheric chemistry evaluation, J. Geophys. Res.-Atmos., 109, D04314, doi:10.1029/2003jd003957, 2004.

Huang, J., Golombek, A., Prinn, R., Weiss, R., Fraser, P., Simmonds, P., Dlugokencky, E. J., Hall, B., Elkins, J., Steele, P., Langenfelds, R., Krummel, P., Dutton, G., and Porter, L.: Estimation of regional emissions of nitrous oxide from 1997 to 2005 using multinetwork measurements, a chemical transport model, and an inverse method, J. Geophys. Res.-Atmos., 113, D17313, doi:10.1029/2007JD009381, 2008.

IPCC: Climate Change 2013: The Physical Science Basis. Contribution of Working Group I to the Fifth Assessment Report of the Intergovernmental Panel on Climate Change, Cambridge University Press, Cambridge, 2013.

IPCC: Climate Change 2014: Impacts, Adaptation, and Vulnerability. Part A: Global and Sectoral Aspects. Contribution of Working Group II to the Fifth Assessment Report of the Intergovernmental Panel on Climate Change, edited by: Field, C. B., Barros, V. R., Dokken, D. J., Mach, K. J., Mastrandrea, M. D., Bilir, T. E., Chatterjee, M., Ebi, K. L., Estrada, Y. O., Genova, R. C., Girma, B., Kissel, E. S., Levy, A. N., MacCracken, S., Mastrandrea, P. R., and White, L. L., Cambridge University Press, Cambridge, United Kingdom and New York, NY, USA, 2014a.

IPCC: Climate Change 2014: Impacts, Adaptation, and Vulnerability. Part B: Regional Aspects. Contribution of Working Group II to the Fifth Assessment Report of the Intergovernmental Panel on Climate Change, edited by: Barros, V. R., Field, C. B., Dokken, D. J., Mastrandrea, M. D., Mach, K. J., Bilir, T. E., Chatterjee, M., Ebi, K. L., Estrada, Y. O., Genova, R. C., Girma, B., Kissel, E. S., Levy, A. N., MacCracken, S., Mastrandrea, P. R., and White, L. L., Cambridge University Press, Cambridge, United Kingdom and New York, NY, USA, 2014b.

Jiang, J. H., Livesey, N. J., Su, H., Neary, L., McConnell, J. C., and Richards, N. A. D.: Connecting surface emissions, convective uplifting, and long-range transport of carbon monoxide in the upper troposphere: New observations from the Aura Microwave Limb Sounder, Geophys. Res. Lett., 34, L18812, doi:10.1029/2007gl030638, 2007a.

Jiang, X., Ku, W. L., Shia, R.-L., Li, Q., Elkins, J. W., Prinn, R. G., and Yung, Y. L.: Seasonal cycle of N_2O: Analysis of data, Global Biogeochem. Cy., 21, GB1006, doi:10.1029/2006gb002691, 2007b.

Jordan, A. and Steinberg, B.: Calibration of atmospheric hydrogen measurements, Atmos. Meas. Tech., 4, 509–521, doi:10.5194/amt-4-509-2011, 2011.

Kaiser, J. W., Heil, A., Andreae, M. O., Benedetti, A., Chubarova, N., Jones, L., Morcrette, J.-J., Razinger, M., Schultz, M. G., Suttie, M., and van der Werf, G. R.: Biomass burning emissions estimated with a global fire assimilation system based on observed fire radiative power, Biogeosciences, 9, 527–554, doi:10.5194/bg-9-527-2012, 2012.

Kaplan, J. O., Folberth, G., and Hauglustaine, D. A.: Role of methane and biogenic volatile organic compound sources in late glacial and Holocene fluctuations of atmospheric methane concentrations, Global Biogeochem. Cy., 20, GB2016, doi:10.1029/2005GB002590, 2006.

Kasischke, E. S., Hyer, E. J., Novelli, P. C., Bruhwiler, L. P., French, N. H. F., Sukhinin, A. I., Hewson, J. H., and Stocks, B. J.: Influences of boreal fire emissions on Northern Hemisphere atmospheric carbon and carbon monoxide, Global Biogeochem. Cy., 19, GB1012, doi:10.1029/2004gb002300, 2005.

King, A. W., Andres, R. J., Davis, K. J., Hafer, M., Hayes, D. J., Huntzinger, D. N., de Jong, B., Kurz, W. A., McGuire, A. D., Vargas, R., Wei, Y., West, T. O., and Woodall, C. W.: North America's net terrestrial CO_2 exchange with the atmosphere 1990–2009, Biogeosciences, 12, 399–414, doi:10.5194/bg-12-399-2015, 2015.

Konovalov, I. B., Berezin, E. V., Ciais, P., Broquet, G., Beekmann, M., Hadji-Lazaro, J., Clerbaux, C., Andreae, M. O., Kaiser, J. W., and Schulze, E.-D.: Constraining CO_2 emissions from open biomass burning by satellite observations of co-emitted species: a method and its application to wildfires in Siberia, Atmos. Chem. Phys., 14, 10383–10410, doi:10.5194/acp-14-10383-2014, 2014.

Krishnamurti, T. N., Biswas, M. K., and Rao, D. V. B.: Vertical extension of the Tibetan high of the Asian summer monsoon, Tellus A, 60, 1038–1052, doi:10.1111/j.1600-0870.2008.00359.x, 2008.

Kumar, R., Naja, M., Venkataramani, S., and Wild, O.: Variations in surface ozone at Nainital: A high-altitude site in the central Himalayas, J. Geophys. Res.-Atmos., 115, D16302, doi:10.1029/2009jd013715, 2010.

Kurokawa, J., Ohara, T., Morikawa, T., Hanayama, S., Janssens-Maenhout, G., Fukui, T., Kawashima, K., and Akimoto, H.: Emissions of air pollutants and greenhouse gases over Asian regions during 2000–2008: Regional Emission inventory in ASia (REAS) version 2, Atmos. Chem. Phys., 13, 11019–11058, doi:10.5194/acp-13-11019-2013, 2013.

Lai, S. C., Baker, A. K., Schuck, T. J., van Velthoven, P., Oram, D. E., Zahn, A., Hermann, M., Weigelt, A., Slemr, F., Brenninkmeijer, C. A. M., and Ziereis, H.: Pollution events observed during CARIBIC flights in the upper troposphere between South China and the Philippines, Atmos. Chem. Phys., 10, 1649–1660, doi:10.5194/acp-10-1649-2010, 2010.

Lal, S., Chandra, N., and Venkataramani, S.: A study of CO_2 and related trace gases using a laser based technique at an urban site in western India, Curr. Sci., accepted, 2015.

Langenfelds, R. L., Francey, R. J., Pak, B. C., Steele, L. P., Lloyd, J., Trudinger, C. M., and Allison, C. E.: Interannual growth rate variations of atmospheric CO_2 and its $\delta^{13}C$, H_2, CH_4, and CO between 1992 and 1999 linked to biomass burning, Global Biogeochem. Cy., 16, 1048, doi:10.1029/2001gb001466, 2002.

Lawrence, M. G. and Lelieveld, J.: Atmospheric pollutant outflow from southern Asia: a review, Atmos. Chem. Phys., 10, 11017–11096, doi:10.5194/acp-10-11017-2010, 2010.

Lelieveld, J., Crutzen, P. J., Ramanathan, V., Andreae, M. O., Brenninkmeijer, C. A. M., Campos, T., Cass, G. R., Dickerson, R. R., Fischer, H., de Gouw, J. A., Hansel, A., Jefferson, A., Kley, D., de Laat, A. T. J., Lal, S., Lawrence, M. G., Lobert, J. M., Mayol-Bracero, O. L., Mitra, A. P., Novakov, T., Oltmans, S. J., Prather, K. A., Reiner, T., Rodhe, H., Scheeren, H. A., Sikka, D., and Williams, J.: The Indian Ocean Experiment: Widespread Air Pollution from South and Southeast Asia, Science, 291, 1031–1036, 2001.

Le Quéré, C., Moriarty, R., Andrew, R. M., Peters, G. P., Ciais, P., Friedlingstein, P., Jones, S. D., Sitch, S., Tans, P., Arneth, A., Boden, T. A., Bopp, L., Bozec, Y., Canadell, J. G., Chini, L. P., Chevallier, F., Cosca, C. E., Harris, I., Hoppema, M., Houghton, R. A., House, J. I., Jain, A. K., Johannessen, T., Kato, E., Keeling, R. F., Kitidis, V., Klein Goldewijk, K., Koven, C., Landa, C. S., Landschützer, P., Lenton, A., Lima, I. D., Marland, G., Mathis, J. T., Metzl, N., Nojiri, Y., Olsen, A., Ono, T., Peng, S., Peters, W., Pfeil, B., Poulter, B., Raupach, M. R., Regnier, P., Rödenbeck, C., Saito, S., Salisbury, J. E., Schuster, U., Schwinger, J., Séférian, R., Segschneider, J., Steinhoff, T., Stocker, B. D., Sutton, A. J., Takahashi, T., Tilbrook, B., van der Werf, G. R., Viovy, N., Wang, Y.-P., Wanninkhof, R., Wiltshire, A., and Zeng, N.: Global carbon budget 2014, Earth Syst. Sci. Data, 7, 47–85, doi:10.5194/essd-7-47-2015, 2015.

Levin, I., Ciais, P., Langenfelds, R., Schmidt, M., Ramonet, M., Sidorov, K., Tchebakova, N., Gloor, M., Heimann, M., Schulze, E. D., Vygodskaya, N. N., Shibistova, O., and Lloyd, J.: Three years of trace gas observations over the EuroSiberian domain derived from aircraft sampling — a concerted action, Tellus B, 54, 696–712, doi:10.1034/j.1600-0889.2002.01352.x, 2002.

Li, Q., Jiang, J. H., Wu, D. L., Read, W. G., Livesey, N. J., Waters, J. W., Zhang, Y., Wang, B., Filipiak, M. J., Davis, C. P., Turquety, S., Wu, S., Park, R. J., Yantosca, R. M., and Jacob, D. J.: Convective outflow of South Asian pollution: A global CTM simulation compared with EOS MLS observations, Geophys. Res. Lett., 32, L14826, doi:10.1029/2005gl022762, 2005.

Liao, T., Camp, C. D., and Yung, Y. L.: The seasonal cycle of N_2O, Geophys. Res. Lett., 31, L17108, doi:10.1029/2004gl020345, 2004.

Logan, J. A., Prather, M. J., Wofsy, S. C., and McElroy, M. B.: Tropospheric chemistry: A global perspective, J. Geophys. Res.-Oceans, 86, 7210–7254, doi:10.1029/JC086iC08p07210, 1981.

Lopez, M.: Estimation des émissions de gaz à effet de serre à différentes échelles en France à l'aide d'observations de haute précision, PhD, Université Paris-Sud, 2012.

Luyssaert, S., Abril, G., Andres, R., Bastviken, D., Bellassen, V., Bergamaschi, P., Bousquet, P., Chevallier, F., Ciais, P., Corazza, M., Dechow, R., Erb, K.-H., Etiope, G., Fortems-Cheiney, A., Grassi, G., Hartmann, J., Jung, M., Lathière, J., Lohila, A., Mayorga, E., Moosdorf, N., Njakou, D. S., Otto, J., Papale, D., Peters, W., Peylin, P., Raymond, P., Rödenbeck, C., Saarnio, S., Schulze, E.-D., Szopa, S., Thompson, R., Verkerk, P. J., Vuichard, N., Wang, R., Wattenbach, M., and Zaehle, S.: The European land and inland water CO_2, CO, CH_4 and N_2O balance between 2001 and 2005, Biogeosciences, 9, 3357–3380, doi:10.5194/bg-9-3357-2012, 2012.

Machida, T., Matsueda, H., Sawa, Y., Nakagawa, Y., Hirotani, K., Kondo, N., Goto, K., Nakazawa, T., Ishikawa, K., and Ogawa, T.: Worldwide Measurements of Atmospheric CO_2 and Other Trace Gas Species Using Commercial Airlines, J. Atmos. Ocean. Tech., 25, 1744–1754, doi:10.1175/2008jtecha1082.1, 2008.

Maiss, M., Steele, L. P., Francey, R. J., Fraser, P. J., Langenfelds, R. L., Trivett, N. B. A., and Levin, I.: Sulfur hexafluoride – A powerful new atmospheric tracer, Atmos. Environ., 30, 1621–1629, doi:10.1016/1352-2310(95)00425-4, 1996.

Matthews, E., Fung, I., and Lerner, J.: Methane emission from rice cultivation: Geographic and seasonal distribution of cultivated areas and emissions, Global Biogeochem. Cy., 5, 3–24, doi:10.1029/90GB02311, 1991.

Mauzerall, D. L., Logan, J. A., Jacob, D. J., Anderson, B. E., Blake, D. R., Bradshaw, J. D., Heikes, B., Sachse, G. W., Singh, H., and Talbot, B.: Photochemistry in biomass burning plumes and implications for tropospheric ozone over the tropical South Atlantic, J. Geophys. Res.-Atmos., 103, 8401–8423, doi:10.1029/97jd02612, 1998.

Messager, C.: Estimation des flux de gaz à effet de serre à l'échelle régionale à partir de mesures atmosphériques, Université Paris 7 – Denis Diderot, 2007.

Ministry of Environment and Forests, Government of India (MoEF): India Second National Communication to the United Nations Framework Convention on Climate Change, New Delhia, available at: http://unfccc.int/resource/docs/natc/indnc2.pdf (last access: 1 August 2015), 2012.

Minschwaner, K., Salawitch, R. J., and McElroy, M. B.: Absorption of solar radiation by O_2: Implications for O_3 and lifetimes of N_2O, $CFCl_3$, and CF_2Cl_2, J. Geophys. Res.-Atmos., 98, 10543–10561, doi:10.1029/93jd00223, 1993.

Montzka, S. A., Dlugokencky, E. J., and Butler, J. H.: Non-CO_2 greenhouse gases and climate change, Nature, 476, 43–50, 2011.

Moorthy, K. K., Sreekanth, V., Chaubey, J. P., Gogoi, M. M., Babu, S. S., Kompalli, S. K., Bagare, S. P., Bhatt, B. C., Gaur, V. K., Prabhu, T. P., Singh, N. S.: Fine and ultrafine particles at near-free tropospheric environment over the high-altitude station Hanle in the Trans-Himalaya: New particle formation and size distribution, J. Geophys. Res.-Atmos., 116, D20212, doi:10.1029/2011JD016343, 2011

Morgan, C. G., Allen, M., Liang, M. C., Shia, R. L., Blake, G. A., and Yung, Y. L.: Isotopic fractionation of nitrous oxide in the stratosphere: Comparison between model and observations, J. Geophys. Res.-Atmos., 109, D04305, doi:10.1029/2003jd003402, 2004.

Morris, R. A., Miller, T. M., Viggiano, A. A., Paulson, J. F., Solomon, S., and Reid, G.: Effects of electron and ion reactions on atmospheric lifetimes of fully fluorinated compounds, J. Geophys. Res.-Atmos., 100, 1287–1294, doi:10.1029/94jd02399, 1995.

Mühle, J., Brenninkmeijer, C. A. M., Rhee, T. S., Slemr, F., Oram, D. E., Penkett, S. A., and Zahn, A.: Biomass burning and fossil fuel signatures in the upper troposphere observed during a

CARIBIC flight from Namibia to Germany, Geophys. Res. Lett., 29, 1910, doi:10.1029/2002gl015764, 2002.

Niwa, Y., Machida, T., Sawa, Y., Matsueda, H., Schuck, T. J., Brenninkmeijer, C. A. M., Imasu, R., and Satoh, M.: Imposing strong constraints on tropical terrestrial CO_2 fluxes using passenger aircraft based measurements, J. Geophys. Res.-Atmos., 117, D11303, doi:10.1029/2012jd017474, 2012.

Niwa, Y., Tsuboi, K., Matsueda, H., Sawa, Y., Machida, T., Nakamura, M., Kawasato, T., Saito, K., Takatsuji, S., Tsuji, K., Nishi, H., Dehara, K., Baba, Y., Kuboike, D., Iwatsubo, S., Ohmori, H., and Hanamiya, Y.: Seasonal Variations of CO_2, CH_4, N_2O and CO in the Mid-Troposphere over the Western North Pacific Observed Using a C-130H Cargo Aircraft, J. Meteor. Soc. Japan. Ser. II, 92, 55–70, doi:10.2151/jmsj.2014-104, 2014.

Novelli, P. C. and Masarie, K. A.: Atmospheric Carbon Monoxide Dry Air Mole Fractions from the NOAA ESRL Carbon Cycle Cooperative Global Air Sampling Network, 1988-2013, Version: 2014-07-02, available at: ftp://aftp.cmdl.noaa.gov/data/trace_gases/co/flask/surface/ (last access: 11 December 2014), 2014.

Novelli, P. C., Steele, L. P., and Tans, P. P.: Mixing ratios of carbon monoxide in the troposphere, J. Geophys. Res.-Atmos., 97, 20731–20750, doi:10.1029/92jd02010, 1992.

Novelli, P. C., Masarie, K. A., and Lang, P. M.: Distributions and recent changes of carbon monoxide in the lower troposphere, J. Geophys. Res.-Atmos., 103, 19015–19033, doi:10.1029/98jd01366, 1998.

Novelli, P. C., Lang, P. M., Masarie, K. A., Hurst, D. F., Myers, R., and Elkins, J. W.: Molecular hydrogen in the troposphere: Global distribution and budget, J. Geophys. Res.-Atmos., 104, 30427–30444, doi:10.1029/1999jd900788, 1999.

Novelli, P. C., Lang, P. M., and Masarie, K. A.: Atmospheric Hydrogen Dry Air Mole Fractions from the NOAA ESRL Carbon Cycle Cooperative Global Air Sampling Network, 1988–2009, Version: 2014-08-27, available at: ftp://aftp.cmdl.noaa.gov/data/trace_gases/h2/flask/surface/ (last access: 11 December 2014), 2014.

Olivier, J. G. J., Van Aardenne, J. A., Dentener, F., Ganzeveld, L., and Peters, J. A. H. W.: Recent trends in global greenhouse gas emissions: regional trends and spatial distribution of key sources, in: Non-CO_2 Greenhouse Gases (NCGG-4), edited by: Van Amstel, A., 325–330, Millpress, Rotterdam, The Netherlands, 2005.

Paris, J. D., Ciais, P., NÉDÉLec, P., Ramonet, M., Belan, B. D., Arshinov, M. Y., Golitsyn, G. S., Granberg, I., Stohl, A., Cayez, G., Athier, G., Boumard, F., and Cousin, J. M.: The YAK-AEROSIB transcontinental aircraft campaigns: new insights on the transport of CO_2, CO and O_3 across Siberia, Tellus B, 60, 551–568, doi:10.1111/j.1600-0889.2008.00369.x, 2008.

Park, M., Randel, W. J., Gettelman, A., Massie, S. T., and Jiang, J. H.: Transport above the Asian summer monsoon anticyclone inferred from Aura Microwave Limb Sounder tracers, J. Geophys. Res.-Atmos., 112, D16309, doi:10.1029/2006jd008294, 2007.

Pathak, H., Bhatia, A., Jain, N., and Aggarwal, P. K.: Greenhouse Gas Emission and Mitigation in Indian Agriculture – A Review, in: ING Bulletins on Regional Assessment of Reactive Nitrogen, Bulletin No. 19, edited by: Singh, B., SCON-ING, New Delhi, i–iv and 1–34, 2010.

Patra, P., Takigawa, M., Ishijima, K., Choi, B.-C., Cunnold, D., J. Dlugokencky, E., Fraser, P., J. Gomez-Pelaez, A., Goo, T.-Y., Kim, J.-S., Krummel, P., Langenfelds, R., Meinhardt, F., Mukai, H., O'Doherty, S., Prinn, R. G., Simmonds, P., Steele, P., Tohjima, Y., Tsuboi, K., Uhse, K., Weiss, R., Worthy, D., and Nakazawa, T.: Growth Rate, Seasonal, Synoptic, Diurnal Variations and Budget of Methane in the Lower Atmosphere, J. Meteor. Soc. Japan. Ser. II, 87, 635–663, 2009.

Patra, P. K., Lal, S., Venkataramani, S., de Sousa, S. N., Sarma, V. V. S. S., and Sardesai, S.: Seasonal and spatial variability in N_2O distribution in the Arabian Sea, Deep Sea Res. Pt. I, 46, 529–543, doi:10.1016/S0967-0637(98)00071-5, 1999.

Patra, P. K., Houweling, S., Krol, M., Bousquet, P., Belikov, D., Bergmann, D., Bian, H., Cameron-Smith, P., Chipperfield, M. P., Corbin, K., Fortems-Cheiney, A., Fraser, A., Gloor, E., Hess, P., Ito, A., Kawa, S. R., Law, R. M., Loh, Z., Maksyutov, S., Meng, L., Palmer, P. I., Prinn, R. G., Rigby, M., Saito, R., and Wilson, C.: TransCom model simulations of CH_4 and related species: linking transport, surface flux and chemical loss with CH_4 variability in the troposphere and lower stratosphere, Atmos. Chem. Phys., 11, 12813–12837, doi:10.5194/acp-11-12813-2011, 2011a.

Patra, P. K., Niwa, Y., Schuck, T. J., Brenninkmeijer, C. A. M., Machida, T., Matsueda, H., and Sawa, Y.: Carbon balance of South Asia constrained by passenger aircraft CO_2 measurements, Atmos. Chem. Phys., 11, 4163–4175, doi:10.5194/acp-11-4163-2011, 2011b.

Patra, P. K., Canadell, J. G., Houghton, R. A., Piao, S. L., Oh, N.-H., Ciais, P., Manjunath, K. R., Chhabra, A., Wang, T., Bhattacharya, T., Bousquet, P., Hartman, J., Ito, A., Mayorga, E., Niwa, Y., Raymond, P. A., Sarma, V. V. S. S., and Lasco, R.: The carbon budget of South Asia, Biogeosciences, 10, 513–527, doi:10.5194/bg-10-513-2013, 2013.

Peylin, P., Law, R. M., Gurney, K. R., Chevallier, F., Jacobson, A. R., Maki, T., Niwa, Y., Patra, P. K., Peters, W., Rayner, P. J., Rödenbeck, C., van der Laan-Luijkx, I. T., and Zhang, X.: Global atmospheric carbon budget: results from an ensemble of atmospheric CO2 inversions, Biogeosciences, 10, 6699–6720, doi:10.5194/bg-10-6699-2013, 2013.

Pison, I., Bousquet, P., Chevallier, F., Szopa, S., and Hauglustaine, D.: Multi-species inversion of CH_4, CO and H_2 emissions from surface measurements, Atmos. Chem. Phys., 9, 5281–5297, doi:10.5194/acp-9-5281-2009, 2009.

Press, W. H., Teukolsky, S. A., Vetterling, W. T., and Flannery, B. P.: Straight-Line Data with Errors in Both Coordinates, in: Numerical Recipes: The Art of Scientific Computing, Cambridge University Press, New York, pp. 785–788, 2007.

Price, H., Jaeglé, L., Rice, A., Quay, P., Novelli, P. C., and Gammon, R.: Global budget of molecular hydrogen and its deuterium content: Constraints from ground station, cruise, and aircraft observations, J. Geophys. Res.-Atmos., 112, D22108, doi:10.1029/2006jd008152, 2007.

Ramonet, M., Ciais, P., Nepomniachii, I., Sidorov, K., Neubert, R. E. M., Langendörfer, U., Picard, D., Kazan, V., Biraud, S., Gusti, M., Kolle, O., Schulze, E. D., and Lloyd, J.: Three years of aircraft-based trace gas measurements over the Fyodorovskoye southern taiga forest, 300 km north-west of Moscow, Tellus B, 54, 713–734, doi:10.1034/j.1600-0889.2002.01358.x, 2002.

Randel, W. J. and Park, M.: Deep convective influence on the Asian summer monsoon anticyclone and associated tracer variability observed with Atmospheric Infrared Sounder (AIRS), J. Geo-

phys. Res.-Atmos., 111, D12314, doi:10.1029/2005JD006490, 2006.

Ravishankara, A. R., Daniel, J. S., and Portmann, R. W.: Nitrous oxide (N_2O): The dominant ozone-depleting substance emitted in the 21st century, Science, 326, 123–125, doi:10.1126/science.1176985, 2009.

Ravishankara, A. R., Solomon, S., Turnipseed, A. A., and Warren, R. F.: Atmospheric lifetimes of long-lived halogenated species, Science, 259, 194–199, 1993.

Rayner, P. J., Law, R. M., Allison, C. E., Francey, R. J., Trudinger, C. M., and Pickett-Heaps, C.: Interannual variability of the global carbon cycle (1992–2005) inferred by inversion of atmospheric CO_2 and $\delta^{13}CO_2$ measurements, Global Biogeochem. Cy., 22, GB3008, doi:10.1029/2007gb003068, 2008.

R Core Team: R: A language and environment for statistical computing. R Foundation for Statistical computing, Vienna, Austria, available at: http://www.r-project.org/, last access: 13 September 2014.

Rivier, L., Ciais, P., Hauglustaine, D. A., Bakwin, P., Bousquet, P., Peylin, P., and Klonecki, A.: Evaluation of SF_6, C_2Cl_4, and CO to approximate fossil fuel CO_2 in the Northern Hemisphere using a chemistry transport model, J. Geophys. Res.-Atmos., 111, D16311, doi:10.1029/2005jd006725, 2006.

Saikawa, E., Prinn, R. G., Dlugokencky, E., Ishijima, K., Dutton, G. S., Hall, B. D., Langenfelds, R., Tohjima, Y., Machida, T., Manizza, M., Rigby, M., O'Doherty, S., Patra, P. K., Harth, C. M., Weiss, R. F., Krummel, P. B., van der Schoot, M., Fraser, P. J., Steele, L. P., Aoki, S., Nakazawa, T., and Elkins, J. W.: Global and regional emissions estimates for N_2O, Atmos. Chem. Phys., 14, 4617–4641, doi:10.5194/acp-14-4617-2014, 2014.

Sawa, Y., Matsueda, H., Makino, Y., Inoue, H. Y., Murayama, S., Hirota, M., Tsutsumi, Y., Zaizen, Y., Ikegami, M., and Okada, K.: Aircraft Observation of CO_2, CO, O_3 and H_2 over the North Pacific during the PACE-7 Campaign, Tellus B, 56, 2–20, doi:10.1111/j.1600-0889.2004.00088.x, 2004.

Schuck, T. J., Brenninkmeijer, C. A. M., Baker, A. K., Slemr, F., von Velthoven, P. F. J., and Zahn, A.: Greenhouse gas relationships in the Indian summer monsoon plume measured by the CARIBIC passenger aircraft, Atmos. Chem. Phys., 10, 3965–3984, doi:10.5194/acp-10-3965-2010, 2010.

Schuck, T. J., Ishijima, K., Patra, P. K., Baker, A. K., Machida, T., Matsueda, H., Sawa, Y., Umezawa, T., Brenninkmeijer, C. A. M., and Lelieveld, J.: Distribution of methane in the tropical upper troposphere measured by CARIBIC and CONTRAIL aircraft, J. Geophys. Res.-Atmos., 117, D19304, doi:10.1029/2012jd018199, 2012.

Seinfeld, J. H. and Pandis, S. N.: Atmospheric Chemistry and Physics: From Air Pollution to Climate Change, John Wiley and Sons, Hoboken, New Jersey, USA, 2006.

Sivakumar, I. and Anitha, M.: Education and girl children in Puducherry region: Problems and perspective, Int. J. Soc. Sci. Interdiscipl. Res., 1, 175–184, 2012.

Streets, D. G., Bond, T. C., Carmichael, G. R., Fernandes, S. D., Fu, Q., He, D., Klimont, Z., Nelson, S. M., Tsai, N. Y., Wang, M. Q., Woo, J. H., and Yarber, K. F.: An inventory of gaseous and primary aerosol emissions in Asia in the year 2000, J. Geophys. Res.-Atmos., 108, 8809, doi:10.1029/2002jd003093, 2003a.

Streets, D. G., Yarber, K. F., Woo, J. H., and Carmichael, G. R.: Biomass burning in Asia: Annual and seasonal estimates and atmospheric emissions, Global Biogeochem. Cy., 17, 1099, doi:10.1029/2003gb002040, 2003b.

Suntharalingam, P., Jacob, D. J., Palmer, P. I., Logan, J. A., Yantosca, R. M., Xiao, Y., Evans, M. J., Streets, D. G., Vay, S. L., and Sachse, G. W.: Improved quantification of Chinese carbon fluxes using CO_2/CO correlations in Asian outflow, J. Geophys. Res.-Atmos., 109, D18S18, doi:10.1029/2003jd004362, 2004.

Swathi, P. S., Indira, N. K., Rayner, P. J., Ramonet, M., Jagadheesha, D., Bhatt, B. C., and Gaur, V. K.: Robust inversion of carbon dioxide fluxes over temperate Eurasia in 2006–2008, Curr. Sci., 105, 201–208, 2013.

Takegawa, N., Kondo, Y., Koike, M., Chen, G., Machida, T., Watai, T., Blake, D. R., Streets, D. G., Woo, J. H., Carmichael, G. R., Kita, K., Miyazaki, Y., Shirai, T., Liley, J. B., and Ogawa, T.: Removal of NO_x and NO_y in Asian outflow plumes: Aircraft measurements over the western Pacific in January 2002, J. Geophys. Res.-Atmos., 109, D23S04, doi:10.1029/2004jd004866, 2004.

Teetor, P.: Performing Simple Orthogonal Regression, in: R Cookbook, edited by: Loukides, M., O'Reilly Media, Sebastopol, 340–341, 2011.

Thompson, R. L., Chevallier, F., Crotwell, A. M., Dutton, G., Langenfelds, R. L., Prinn, R. G., Weiss, R. F., Tohjima, Y., Nakazawa, T., Krummel, P. B., Steele, L. P., Fraser, P., O'Doherty, S., Ishijima, K., and Aoki, S.: Nitrous oxide emissions 1999 to 2009 from a global atmospheric inversion, Atmos. Chem. Phys., 14, 1801–1817, doi:10.5194/acp-14-1801-2014, 2014a.

Thompson, R. L., Ishijima, K., Saikawa, E., Corazza, M., Karstens, U., Patra, P. K., Bergamaschi, P., Chevallier, F., Dlugokencky, E., Prinn, R. G., Weiss, R. F., O'Doherty, S., Fraser, P. J., Steele, L. P., Krummel, P. B., Vermeulen, A., Tohjima, Y., Jordan, A., Haszpra, L., Steinbacher, M., Van der Laan, S., Aalto, T., Meinhardt, F., Popa, M. E., Moncrieff, J., and Bousquet, P.: TransCom N_2O model inter-comparison – Part 2: Atmospheric inversion estimates of N_2O emissions, Atmos. Chem. Phys., 14, 6177–6194, doi:10.5194/acp-14-6177-2014, 2014b.

Thompson, R. L., Patra, P. K., Ishijima, K., Saikawa, E., Corazza, M., Karstens, U., Wilson, C., Bergamaschi, P., Dlugokencky, E., Sweeney, C., Prinn, R. G., Weiss, R. F., O'Doherty, S., Fraser, P. J., Steele, L. P., Krummel, P. B., Saunois, M., Chipperfield, M., and Bousquet, P.: TransCom N_2O model inter-comparison – Part 1: Assessing the influence of transport and surface fluxes on tropospheric N_2O variability, Atmos. Chem. Phys., 14, 4349–4368, doi:10.5194/acp-14-4349-2014, 2014c.

Thoning, K. W., Tans, P. P., and Komhyr, W. D.: Atmospheric carbon dioxide at Mauna Loa Observatory: 2. Analysis of the NOAA GMCC data, 1974–1985, J. Geophys. Res.-Atmos., 94, 8549–8565, doi:10.1029/JD094iD06p08549, 1989.

Tiwari, Y. K. and Kumar, K. R.: GHG observation programs in India, in: Asian GAW greenhouse gases Newsletter, Volume No. 3, Korea Meteorological Administration, Chungnam, South Korea, 2012.

Tiwari, Y. K., Patra, P. K., Chevallier, F., Francey, R. J., Krummel, P. B., Allison, C. E., Revadekar, J. V., Chakraborty, S., Langenfelds, R. L., Bhattacharya, S. K., Borole, D. V., Kumar, K. R., and Steele, L. P.: Carbon dioxide observations at Cape Rama, India for the period 1993–2002: implications for constraining Indian emissions, Curr. Sci., 101, 1562–1568, 2011.

Tiwari, Y. K., Revadekar, J. V., and Ravi Kumar, K.: Variations in atmospheric Carbon Dioxide and its association with rainfall and vegetation over India, Atmos. Environ., 68, 45–51, doi:10.1016/j.atmosenv.2012.11.040, 2013.

Tiwari, Y. K., Vellore, R. K., Ravi Kumar, K., van der Schoot, M., and Cho, C.-H.: Influence of monsoons on atmospheric CO_2 spatial variability and ground-based monitoring over India, Sci. Total Environ., 490, 570–578, doi:10.1016/j.scitotenv.2014.05.045, 2014.

Tohjima, Y., Maksyutov, S., Machida, T., and Inoue, G.: Airborne measurements of atmospheric methane over oil fields in western Siberia, Geophys. Res. Lett., 23, 1621–1624, doi:10.1029/96gl01027, 1996.

Turnbull, J. C., Miller, J. B., Lehman, S. J., Tans, P. P., Sparks, R. J., and Southon, J.: Comparison of 14CO2, CO, and SF6 as tracers for recently added fossil fuel CO2 in the atmosphere and implications for biological CO_2 exchange, Geophys. Res. Lett., 33, L01817, doi:10.1029/2005gl024213, 2006.

Valsala, V., Tiwari, Y. K., Pillai, P., Roxy, M., Maksyutov, S., and Murtugudde, R.: Intraseasonal variability of terrestrial biospheric CO_2 fluxes over India during summer monsoons, J. Geophys. Res.-Biogeo., 118, 752–769, doi:10.1002/jgrg.20037, 2013.

van der Werf, G. R., Randerson, J. T., Giglio, L., Collatz, G. J., Kasibhatla, P. S., and Arellano Jr., A. F.: Interannual variability in global biomass burning emissions from 1997 to 2004, Atmos. Chem. Phys., 6, 3423–3441, doi:10.5194/acp-6-3423-2006, 2006.

van der Werf, G. R., Randerson, J. T., Giglio, L., Collatz, G. J., Mu, M., Kasibhatla, P. S., Morton, D. C., DeFries, R. S., Jin, Y., and van Leeuwen, T. T.: Global fire emissions and the contribution of deforestation, savanna, forest, agricultural, and peat fires (1997–2009), Atmos. Chem. Phys., 10, 11707–11735, doi:10.5194/acp-10-11707-2010, 2010.

Venkataraman, C., Habib, G., Eiguren-Fernandez, A., Miguel, A. H., and Friedlander, S. K.: Residential Biofuels in South Asia: Carbonaceous Aerosol Emissions and Climate Impacts, Science, 307, 1454–1456, 2005.

Volk, C. M., Elkins, J. W., Fahey, D. W., Dutton, G. S., Gilligan, J. M., Loewenstein, M., Podolske, J. R., Chan, K. R., and Gunson, M. R.: Evaluation of source gas lifetimes from stratospheric observations, J. Geophys. Res.-Atmos., 102, 25543–25564, doi:10.1029/97jd02215, 1997.

Wada, A., Matsueda, H., Sawa, Y., Tsuboi, K., and Okubo, S.: Seasonal variation of enhancement ratios of trace gases observed over 10 years in the western North Pacific, Atmos. Environ., 45, 2129–2137, doi:10.1016/j.atmosenv.2011.01.043, 2011.

Wang, R., Tao, S., Ciais, P., Shen, H. Z., Huang, Y., Chen, H., Shen, G. F., Wang, B., Li, W., Zhang, Y. Y., Lu, Y., Zhu, D., Chen, Y. C., Liu, X. P., Wang, W. T., Wang, X. L., Liu, W. X., Li, B. G., and Piao, S. L.: High-resolution mapping of combustion processes and implications for CO_2 emissions, Atmos. Chem. Phys., 13, 5189–5203, doi:10.5194/acp-13-5189-2013, 2013.

Xiao, Y., Jacob, D. J., Wang, J. S., Logan, J. A., Palmer, P. I., Suntharalingam, P., Yantosca, R. M., Sachse, G. W., Blake, D. R., and Streets, D. G.: Constraints on Asian and European sources of methane from CH_4-C_2H_6-CO correlations in Asian outflow, J. Geophys. Res.-Atmos., 109, D15S16, doi:10.1029/2003jd004475, 2004.

Xiong, X., Houweling, S., Wei, J., Maddy, E., Sun, F., and Barnet, C.: Methane plume over south Asia during the monsoon season: satellite observation and model simulation, Atmos. Chem. Phys., 9, 783–794, doi:10.5194/acp-9-783-2009, 2009.

Yan, X., Cai, Z., Ohara, T., and Akimoto, H.: Methane emission from rice fields in mainland China: Amount and seasonal and spatial distribution, J. Geophys. Res.-Atmos., 108, 4505, doi:10.1029/2002jd003182, 2003.

Yashiro, H., Sudo, K., Yonemura, S., and Takigawa, M.: The impact of soil uptake on the global distribution of molecular hydrogen: chemical transport model simulation, Atmos. Chem. Phys., 11, 6701–6719, doi:10.5194/acp-11-6701-2011, 2011.

Yevich, R. and Logan, J. A.: An assessment of biofuel use and burning of agricultural waste in the developing world, Global Biogeochem. Cy., 17, 1095, doi:10.1029/2002gb001952, 2003.

Yver, C.: Estimation des sources et puits du dihydrogène troposphérique – développements instrumentaux, mesures atmosphériques et assimilation variationnelle, PhD dissertation, Université de Versailles – Saint Quentin, 2010.

Yver, C., Schmidt, M., Bousquet, P., Zahorowski, W., and Ramonet, M.: Estimation of the molecular hydrogen soil uptake and traffic emissions at a suburban site near Paris through hydrogen, carbon monoxide, and radon-222 semicontinuous measurements, J. Geophys. Res.-Atmos., 114, D18304, doi:10.1029/2009jd012122, 2009.

Yver, C. E., Pison, I. C., Fortems-Cheiney, A., Schmidt, M., Chevallier, F., Ramonet, M., Jordan, A., Søvde, O. A., Engel, A., Fisher, R. E., Lowry, D., Nisbet, E. G., Levin, I., Hammer, S., Necki, J., Bartyzel, J., Reimann, S., Vollmer, M. K., Steinbacher, M., Aalto, T., Maione, M., Arduini, J., O'Doherty, S., Grant, A., Sturges, W. T., Forster, G. L., Lunder, C. R., Privalov, V., Paramonova, N., Werner, A., and Bousquet, P.: A new estimation of the recent tropospheric molecular hydrogen budget using atmospheric observations and variational inversion, Atmos. Chem. Phys., 11, 3375–3392, doi:10.5194/acp-11-3375-2011, 2011.

Zhang, F., Zhou, L. X., Novelli, P. C., Worthy, D. E. J., Zellweger, C., Klausen, J., Ernst, M., Steinbacher, M., Cai, Y. X., Xu, L., Fang, S. X., and Yao, B.: Evaluation of in situ measurements of atmospheric carbon monoxide at Mount Waliguan, China, Atmos. Chem. Phys., 11, 5195–5206, doi:10.5194/acp-11-5195-2011, 2011.

Zhang, H. F., Chen, B. Z., van der Laan-Luijk, I. T., Machida, T., Matsueda, H., Sawa, Y., Fukuyama, Y., Langenfelds, R., van der Schoot, M., Xu, G., Yan, J. W., Cheng, M. L., Zhou, L. X., Tans, P. P., and Peters, W.: Estimating Asian terrestrial carbon fluxes from CONTRAIL aircraft and surface CO_2 observations for the period 2006–2010, Atmos. Chem. Phys., 14, 5807–5824, doi:10.5194/acp-14-5807-2014, 2014.

Zhang, X. I. A., Nakazawa, T., Ishizawa, M., Aoki, S., Nakaoka, S.-I., Sugawara, S., Maksyutov, S., Saeki, T., and Hayasaka, T.: Temporal variations of atmospheric carbon dioxide in the southernmost part of Japan, Tellus B, 59, 654–663, doi:10.1111/j.1600-0889.2007.00288.x, 2007.

Zhao, C. L. and Tans, P. P.: Estimating uncertainty of the WMO mole fraction scale for carbon dioxide in air, J. Geophys. Res.-Atmos., 111, D08S09, doi:10.1029/2005jd006003, 2006.